INL/EXT-08-14746

Computational Fluid Dynamic Analysis for the Proposed VHTR Lower Plenum Standard Problem

R. W. Johnson
W. David Pointer
Richard R. Schultz

September 2008

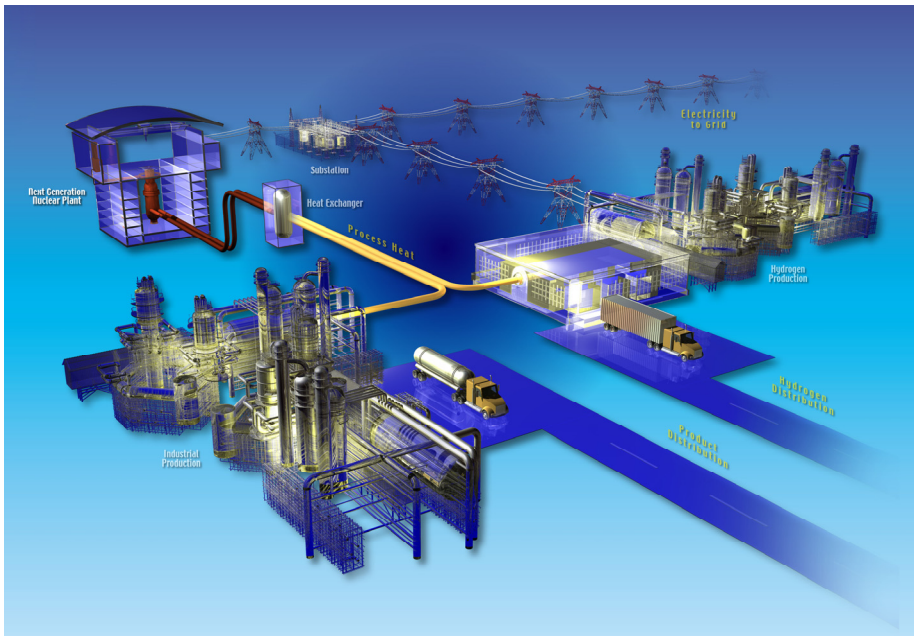

INL/EXT-08-14746

Computational Fluid Dynamic Analysis for the Proposed VHTR Lower Plenum Standard Problem

Richard W. Johnson, W. David Pointer, and Richard R. Schultz

September 2008

Idaho National Laboratory
Idaho Falls, Idaho 83415

Prepared for the
U.S. Department of Energy
Assistant Secretary for Nuclear Energy
Under DOE Idaho Operations Office
Contract DE-AC07-05ID14517

Next Generation Nuclear Plant Project

Computational Fluid Dynamic Analysis for the Proposed VHTR Lower Plenum Standard Problem

INL/EXT-08-14746

September 2008

Approved by:

Richard W. Johnson — 09/24/2008 (Date)

Richard R. Schultz — 9/24/08 (Date)

SUMMARY

One of the reference designs for the Next Generation Nuclear Plant (NGNP) is a prismatic reactor configuration. A major concern in the operation of this design is the nature of the flow of hot gas as it exits the core into the lower plenum and then out the vessel exit duct. The two primary areas of concern are the impingement of hot jets onto the walls of the lower plenum and the degree of thermal mixing of the helium coolant as it flows out of the reactor vessel. Computational fluid dynamic (CFD) simulations have been proposed by general consensus to estimate the desired local fluid dynamic and temperature information.

Successful CFD simulations require careful planning and extensive calculations to help ensure that they accurately represent the flow physics. An important aspect of the application of CFD is to validate the results against detailed validation data, often for scaled problems that involve similar physics. A section of the lower plenum of the reference prismatic NGNP was employed to create a scaled model to use to obtain experimental data for use as validation data for CFD analysis. Figure S-1 provides a drawing of the scaled model that was used to obtain experimental data. Extensive flow data were taken in the scaled model while installed in the INL's Matched Index of Refraction (MIR) test facility.

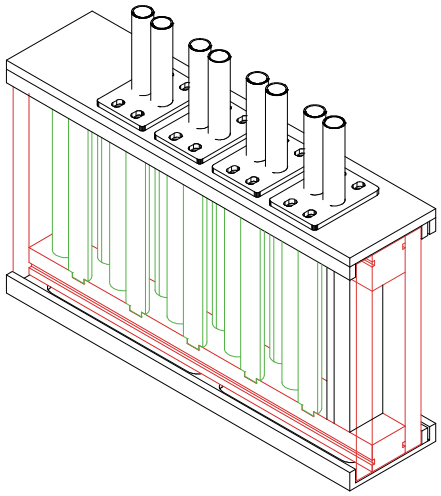

Figure S-1. Drawing of the scaled model used to obtain experimental data for the Standard Problem.

The objective of the present investigation is to raise and sort out issues about the suitability of the scaled model to generate adequate validation data. Some of the issues that may arise include the suitability of the model geometry itself, how many inlet jets should be employed, how sensitive the internal flow is to the symmetry/asymmetry of the inlet jets, how complex the flow actually is, and what issues arise in the details of executing the CFD model. Also, there is the issue of whether a particular commercial CFD code is adequate and practical for the analyses. Other issues are likely to arise during performance of the CFD analysis on the scaled model.

An analysis plan was developed prior to performing the CFD analysis on a 3-D simulation. The analysis determined the most efficient way to address each issue. For example, the effects of using a particular boundary condition in a commercial CFD code can be determined more easily by analyzing it in a 2-D version of the problem, than by applying it to a full 3-D -problem that requires a lengthy compute time.

The overall objective of the analysis plan was to determine the best approach for the numerical analysis that will yield results that most closely represent the physics of the actual flow. This includes a determination of the extent of the computational domain, the most appropriate boundary conditions to use, the fineness of the grid to use, the appropriate tolerance for convergence at each time step, and which turbulence models can be used to compare to the experimental data.

A simplified 2-D-version of the flow was employed to investigate the issues just mentioned. During the development of the analysis plan, it was found that the inclusion of the outer flow around the model is not necessary to obtain adequate numerical representations of the flow field inside the model, but only upstream of the exit. A constant pressure outlet condition, available in commercial CFD codes, provides the best results. In addition, it was found that, for 2-D-models at least, the realizable k~ε turbulence model does not predict vortex shedding. The more sophisticated Reynolds stress turbulence model (RSM), however, does provide for vortex shedding in the flow.

Three-dimensional (3-D)-CFD results were obtained using a mesh containing 14 million cells. The flow was computed for over 1.2 seconds of flow time, taking about 360 hours using 256 computer processors in parallel. The major flow features present in the actual flow, as shown in a flow visualization experiment, are present in the computed flow field. Figure S-2 illustrates a streamline field for the flow at a particular flow time. The streamlines are colored by velocity magnitude. As shown, the highest velocity magnitude occurs at the four inlet jet positions, where the streamlines originate. The flow generally moves downward and later upwards and towards the outlet to the left. Large recirculation regions can be seen below the rightmost jet and between the second and third jets. There is also a region of recirculation and low speed flow just to the left of the fourth jet.

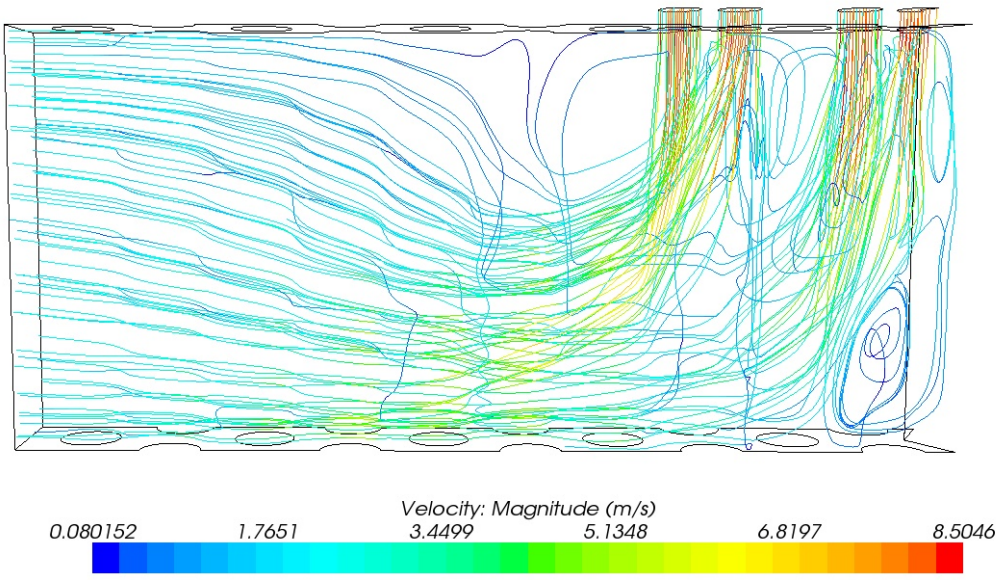

Figure S-2. Streamline field computed for the 3-D field at one point in time. The streamlines are colored by velocity magnitude; flow is right to left. Jets are numbered (first, second, etc.) from right to left.

Figure S-3 is a photograph of a bubble visualization exercise where all four jets are injecting liquid into the physical model, but bubbles are being injected in the rightmost jet along with the liquid. It can be seen that flow patterns similar to the computed patterns in Figure S-2, above, are present. The flow is downward below the jets, then moves horizontally and somewhat upwards toward the exit at the left; there are zones of recirculation at the bottom right and between the two pairs of jets. There is also a large region of low speed flow and recirculation at the top center.

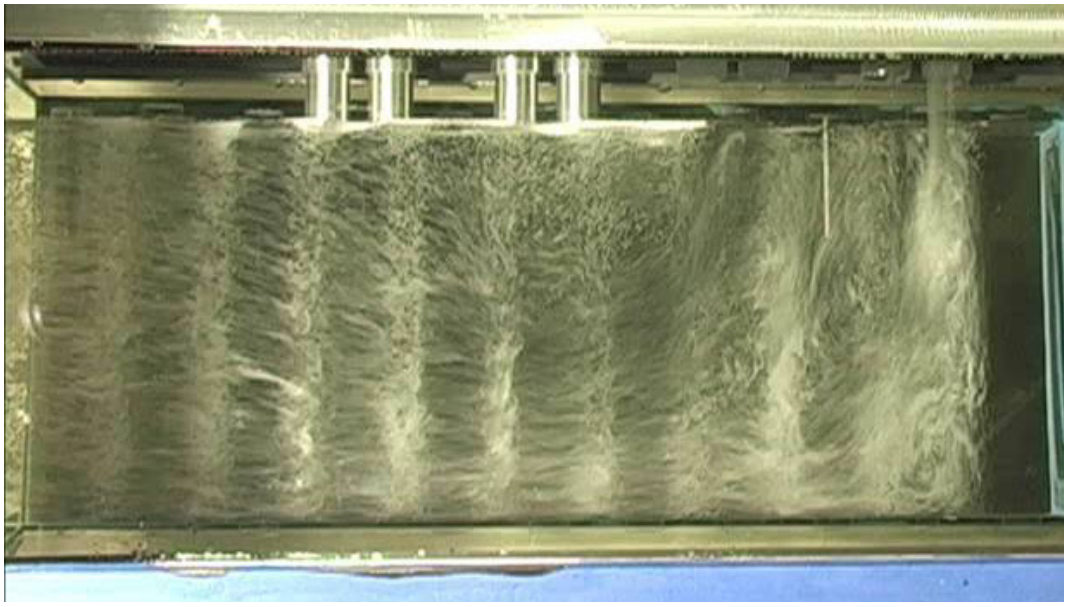

Figure S-3. Photograph of a bubble visualization of the physical model of the Standard Problem. Bubbles are injected into the model through the rightmost jet; flow is right to left.

The 3-D-CFD results exhibit asymmetries that cannot be explained by the inlet profiles (which are uniform) or by the geometry (which is symmetric), but are apparently caused by other subtle influences that may be difficult to control. Figure S-4 illustrates streamwise velocity contours of the long-time averaged flow for a plane about two-thirds of the way from the inlet plane to the bottom of the model. The contours show several instances of asymmetry in the long-time average.

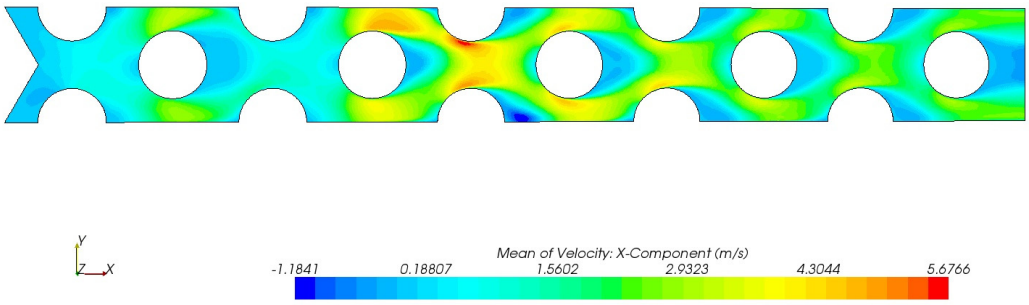

Figure S-4. Long-time averaged (mean) streamwise flow velocity at a plane about two-thirds of the distance from the inlet plane to the bottom of the model. Flow is seen to be asymmetric.

Additional compute time is necessary to determine if suitable long-time averages can be obtained for the flow for comparison with the experimental data. Computations using a coarser mesh would be useful in further investigations into this and other issues. It is also valuable to make computations using data-based inlet profiles to see if sufficient asymmetry is present to avoid excessive sensitivity of the flow to subtle influences.

Several issues were identified that may affect the suitability of the MIR experimental data to be used for a Standard Problem. Also, recommendations addressing these issues are provided below.

Issues that may affect the suitability of the MIR experimental data:

1. When the current geometry is used for the CFD model, there is inflow at the exit to the model. This could be alleviated by extending the outlet of the model without adding any additional cylindrical posts.
2. The physical model is designed to be symmetric. However, 3-D simulations are not symmetric due to a subtle effect of the CFD model. Asymmetry should be built into the model to ensure that subtle influences do not dictate where the flow is asymmetric. It may be very difficult to include such subtle influences in a CFD model.
3. The number of inlet jets should be reduced from four to one. This would decrease the effort needed to set up the CFD model and ensure that any asymmetry built into the model would not be affected by additional jets.

Recommendations for future CFD analysis in relation to a Standard Problem include:

1. Coarser mesh calculations should be made for the 3-D problem to address any remaining issues, such as how long the calculation must run to provide appropriate long-time averages to use for comparison with the Standard Problem data and how asymmetric the flow is because of asymmetric inlet conditions.
2. A series of 3-D grids, varying in degrees of fineness, has been constructed for use with the CFD analysis. These should be employed in comparative simulations to determine which provides the most accurate solutions.
3. The Reynolds number of the present Standard Problem is more than an order of magnitude smaller than the corresponding Reynolds number in the actual lower plenum of the reference VHTR. Calculations at a higher Reynolds number should be made to investigate potential issues associated with the higher value.
4. Computations should be made for any newly proposed design for a Standard Problem to investigate potential issues therein.
5. It is desirable to investigate the application of existing national laboratory CFD software for use in the NGNP because it would provide for control of the software for verification and validation purposes and it could employ better and faster solution algorithms not available in commercial CFD codes.

ACKNOWLEDGEMENTS

This manuscript has been authored by Battelle Energy Alliance, LLC under Contract No. DE-AC07-05ID14517 with the U.S. Department of Energy.

CONTENTS

FIGURES

TABLES

ACRONYMS

ASME	American Society of Mechanical Engineers
CAD	computer-aided design
CFD	computational fluid dynamics
CMVB	computational methods, validation and benchmark
IGES	initial graphics exchange specification (neutral data format)
INL	Idaho National Laboratory (Idaho Falls, Idaho)
MIR	Matched Index of Refraction (INL facility)
NGNP	Next Generation Nuclear Plant
NRC	Nuclear Regulatory Commission
PIRT	phenomena identification and ranking table
PIV	particle image velocimetry
PMB	Project Management Board
RSM	Reynolds stress model (of turbulence)
VHTR	very high temperature reactor

Computational Fluid Dynamic Analysis for the Proposed VHTR Lower Plenum Standard Problem

1. INTRODUCTION

One of the reference designs for the Next Generation Nuclear Plant (NGNP) is a prismatic reactor configuration. A major concern in the operation of this design is the nature of the flow of hot gas as it exits the core into the lower plenum and then out the vessel exit duct. Two primary areas of concern are the impingement of hot jets onto the walls of the lower plenum and the degree of thermal mixing of the helium coolant with spatially varying temperature as it flows out of the reactor vessel. Computational fluid dynamic (CFD) simulations have been proposed by general consensus to estimate the desired local fluid dynamic and temperature information.

Successful CFD simulations require careful planning and extensive calculations to help ensure that they accurately represent the flow physics. An important aspect of the application of CFD is to validate the results against detailed validation data, often for scaled problems that involve similar physics. A scaled section of the lower plenum of the reference prismatic NGNP was employed to create a scaled model to obtain experimental data with the intent to use the data as a validation data set for CFD analysis. Figure 1 provides a plan view of the lower plenum of the reference NGNP indicating likely flow directions; the scaled model was created from a narrow section of the lower plenum (see horizontal arrows) as shown by Figure 2, which is a top view of the scaled model used for the experimental data set.

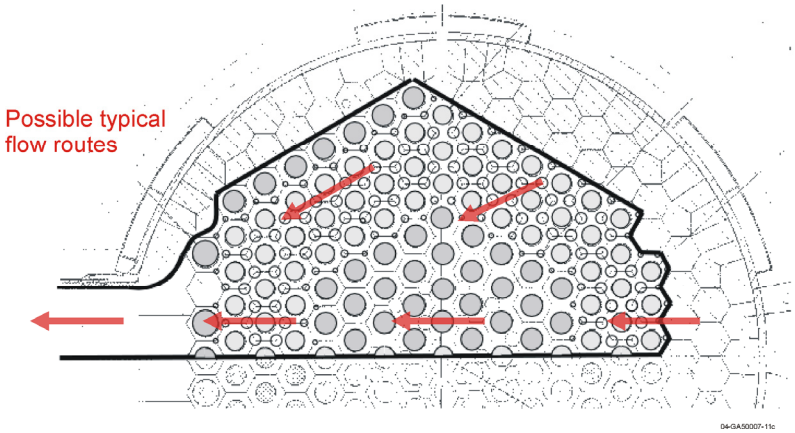

Figure 1. Plan view of the lower plenum of the reference design of the NGNP showing likely flow routes through the lower plenum to the exit duct. Large circles indicate the support columns; smaller circles are the inlet ports for the coolant from the core, and hexagonal blocks are graphite reflectors. The cylindrical support columns hold up hexagonal graphite blocks that constitute the reactor core.

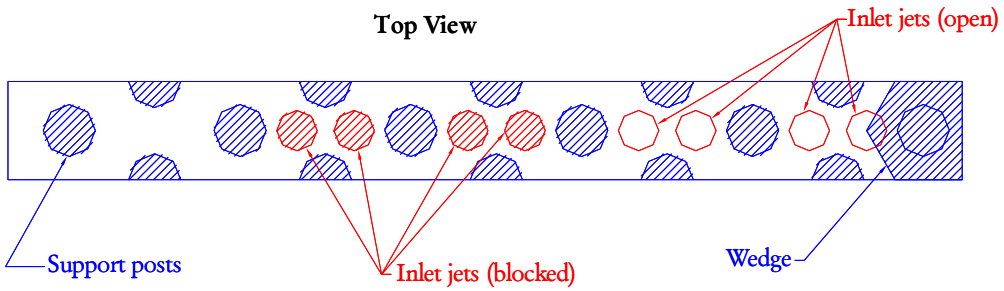

Figure 2. Top view of the scaled model showing full- and half-support posts and inlet jets (ports).

The scaled model includes inlet ports for eight jets, four of which have been blocked. Figure 3 shows a three-dimensional drawing of the scaled model showing the eight inlet ports and the full and half cylinders in the flow section. The sidewalls of the model are 2.54 cm (1 in.) thick. Figure 4 is a photograph of the test section showing the actual inlet port hardware, which includes 90-degree bends in the inlet flow of the mineral oil working fluid. Detailed drawings for the scaled model are provided in Appendix A. Extensive flow data were taken in the scaled model while installed in the INL's Matched Index of Refraction (MIR) test facility.[1]

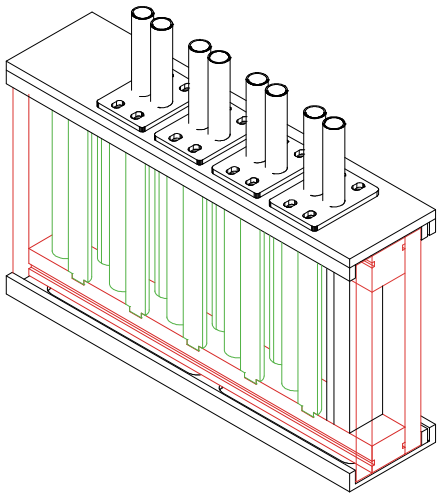

Figure 3. Drawing of the scaled model used in the INL MIR facility to obtain flow data. Flow enters from the top inlets and flows out toward the left rear; half and full cylinders represent core support columns.

Figure 4. Photograph of the scaled model used in the INL MIR facility to obtain flow data. Inlet flow must negotiate a 90º -bend just prior to entering the flow section.

The scaled model was designed without accompanying CFD analysis to raise and sort out issues about the suitability of the model design for use as a validation data set. Some of the issues that may arise include the suitability of the model geometry itself, how many inlet jets should be employed, how

sensitive the internal flow is to the symmetry/asymmetry of the inlet jets, how complex the flow actually is, and how practical it is to solve the CFD model in view of how many cells an appropriate CFD mesh would contain. Also, there is the issue of whether a particular commercial CFD code is adequate and practical to employ for the analyses. Other issues are likely to arise as experience is obtained from performing the CFD analysis on the scaled model. The present study reports the progress in performing a defensible CFD analysis on the scaled model and addresses issues that were foreseen and some that were not, in terms of whether the experimental data for the scaled model represent a suitable and/or useful validation data set.

The CFD analyses described below have been performed in preparation for conducting the first Standard Problem exercise. The idea behind the first exercise is to develop the practices and procedures required for performing multiple Standard Problems in the future, once the NGNP design has been selected. Appendix B outlines the genesis and objectives of the first Standard Problem exercise.

A CFD analysis can greatly benefit from an analysis plan, in particular by addressing issues in more efficient ways than by using brute force to answer them. For example, the effects of using a particular boundary condition in a commercial CFD code can be more easily determined by using it in a much simpler and smaller problem, than by applying it in a full 3-D problem that requires a lengthy compute time. The development of an analysis plan for the unsteady flow that occurs in the 3-D scaled model of a section of the lower plenum is reported next.

2. ANALYSIS PLAN

The overall objective of the analysis plan is to determine the best approach for the numerical analysis that will yield results that most closely represent the physics of the actual flow. This includes a determination of the extent of the computational domain, the most appropriate boundary conditions to use, the fineness of the grid to achieve grid convergence, the appropriate tolerance for iterative convergence at each time step, and which turbulence models can be used to compare to the experimental data.

The first requirement to be applied to the analysis plan is that the CFD code to be used be one that is fully operational and currently and easily available to all interested parties—the National Laboratories, the reactor vendors, and the U.S. Nuclear Regulatory Commission (NRC)—that is, a commercial CFD code. The code used initially for the development of the analysis plan is FLUENT.[2]

An important aspect of the analysis plan is to determine the extent of the computational domain necessary, such that the boundary conditions employed are suitable for the problem computed. The scaled model was installed in the MIR such that the flow medium (mineral oil) flowed both inside and around the outside of the model. It is necessary to know if the outer flow will need to be modeled, along with the inner flow, in order for the present model geometry to produce accurate results. That is, is there a suitable outflow boundary condition that can be used for a CFD model that incorporates only the flow inside the model to allow proper comparisons between calculations and the experimental data?

The scaled model involves flow around several interior posts representing the core block support columns in the lower plenum of the reference prismatic NGNP design. It is expected that the flow will therefore involve shedding vortices at multiple locations as well as turbulence, making the flow nonstationary. It is further desirable to determine which turbulence models are not appropriate for simulating the flow. In fact, it has been found that some two-equation turbulence models do not allow vortex-shedding, probably because of excessive diffusion. Numerical practices employed are based on the ASME Journal of Fluids Engineering "Statement of Numerical Accuracy[3]."

It was deemed appropriate to use a 2-D CFD model of the 3-D scaled model to develop the analysis plan because the geometry of the actual 3-D scaled model is invariant in the third dimension below the plane of the inlet jets. The 2-D CFD model should provide a good idea of how domain considerations and boundary conditions will apply in 3-D. Also, 2-D calculations require far less time than 3-D calculations.

Initial calculations were made using a flow domain that included only the flow region inside the scaled model. Figure 2 above illustrates the cross-section of the scaled model. Flow is from right to left in the scaled model as shown. The final 2-D CFD model was constructed to include some, but not all, of the full and half posts in the scaled model. The last four full posts and the last three pairs of half cylinders were included. Figure 5 illustrates the 2-D CFD model employed for the inner domain CFD model.

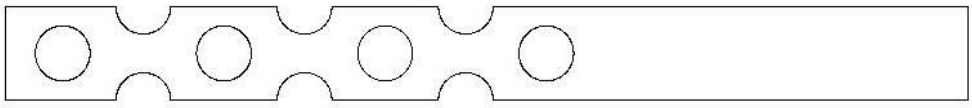

Figure 5. 2-D CFD model for flow inside the scaled model.

Initial 2-D calculations were performed for grid convergence studies using a model similar to that shown in Figure 5, except that only the last two full posts and last two pairs of half posts were included. The realizable two-equation k~ε model employing the enhanced wall treatment was used. The y^+

distribution of the near-wall cell ranged between 0.1 and 6, appropriate to the use of the low Reynolds number wall model approach of the enhanced wall treatment. No vortex shedding could be obtained, even when substantial numerical perturbations were applied to the inlet velocity profile. Again, no vortex shedding was obtained when the wall treatment was changed to standard wall functions (using the same grid); standard wall functions are constructed to be applicable to use in the region very close to the wall.[2]

Vortex shedding was obtained in an earlier numerical study of flow in a tube bundle by the author[3], using the Reynolds stress model (RSM), wherein a separate transport equation is solved for each Reynolds stress. When the RSM was employed in the present study, clear vortex-shedding was obtained, even without any numerical kick applied. The RSM was used throughout the rest of the calculations made in the development of the analysis plan reported herein. While it is not appropriate to determine which turbulence model is most appropriate to simulate the 3-D flow physics until 3-D calculations are made, it appears justified to eliminate the realizable k~ε model from contention inasmuch as it apparently disallows vortex-shedding, probably caused by excessive turbulent diffusion of momentum.

The two clear candidates for outlet boundary conditions in FLUENT are the "outflow" and the "pressure-outlet" conditions. The former enforces a constant gradient condition to the velocity components while the latter sets a constant static pressure condition just downstream of the outlet plane. Actually, neither of these conditions is correct because the outlet to the inner flow domain is just barely downstream of the last full post, such that there is vortex shedding occurring at the outlet plane. It is expected that using just the inner flow for the computational domain is inappropriate; however, it may be the case that numerical simulations for the case of the inner domain only will match simulations for the case that includes the outer domain for some of the region within the inner domain.

Simulations were made using the second-order in space convective-differencing scheme QUICK with second-order implicit time stepping available in FLUENT[2]; the second-order implicit time scheme requires a constant time step. The RSM turbulence model was used with standard wall functions; 'y^+' values ranged from 0.1 to 6. Three grids (a,b,c) were used to investigate grid independence. The grids had 27,232; 67,171; and 113,046 cells. Factors of 1.5 and 1.35 were used on mesh face edges to refine the successive grids. Regions of structured cells were constructed around the posts and half-posts and in the region upstream of the posts. Other regions were paved. Figure 6 provides a close-up of the intermediate grid illustrating its construction.

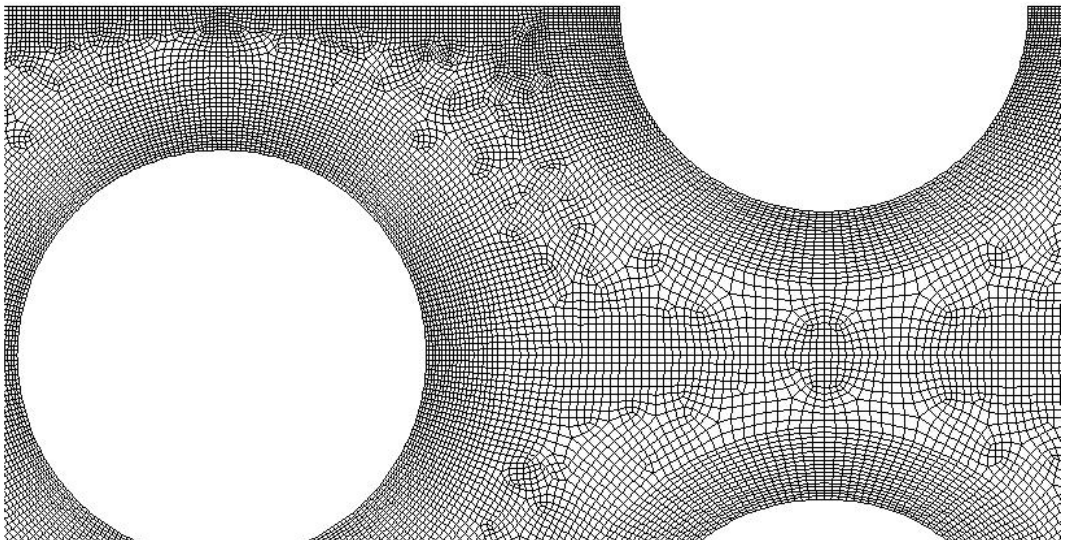

Figure 6. Mesh detail of intermediate grid.

The "pressure-outlet" condition was used at the outlets of the "inside-only" CFD models for the grid study. "Scaled" tolerances[2] of approximately 1×10^{-6} for the velocities and continuity and 1×10^{-5} for turbulence quantities were obtained for the inner iterations. These tolerances were found to be adequate in a related study.[3] A time step of 3.5×10^{-4} sec was used for the coarsest grid; time steps of 1.0×10^{-4} sec were used for the two finer grids. When the time step of 3.5×10^{-4} sec was used for the intermediate mesh, a unique numerical (nonphysical) event occurred. After computing to about 1.57 seconds, the solution changed dramatically with an attendant increase in the residuals of more than an order of magnitude and a proliferation of vortices in a region where there was only one previously. Figure 7 shows a streamline contour plot of the flow just before and just after the event. This is the reason that the time step was decreased to 1×10^{-4} sec, which avoided the occurrence of the event.

Figure 8 shows a time trace for grid "b" for the Reynolds-averaged streamwise velocity "u", which is unsteady because of vortex-shedding, with a symbol at every 5th time step, with a time step of 1.0×10^{-4} sec. The point lies just behind a full post. The time step is fine enough to capture the unsteadiness in the solution. Figure 8 indicates multiple time scales. These are likely caused by multiple vortex-shedding sites.

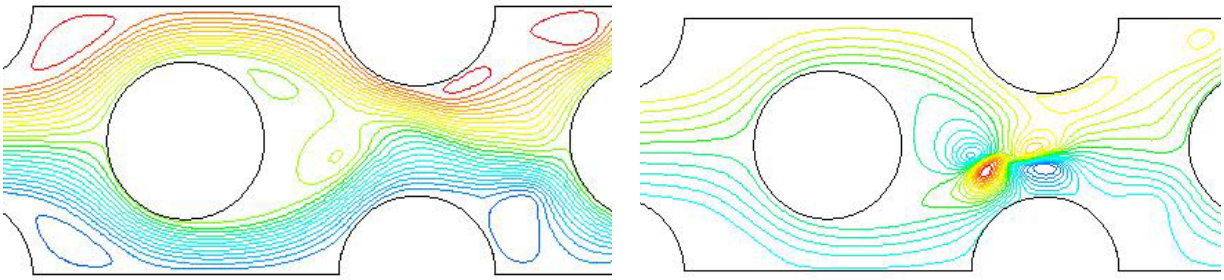

(a) (b)

Figure 7. Stream function contours for the "b" grid (a) just before and (b) just after a nonphysical event because of an excessive time step.

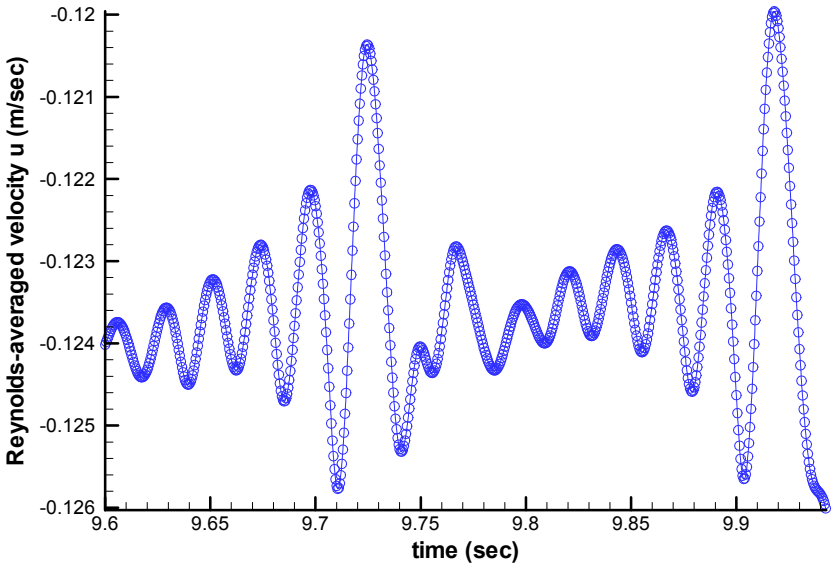

Figure 8. Time trace of the Reynolds-averaged streamwise velocity 'u' for the intermediate grid.

To be able to compare outlet flow conditions between cases, it is necessary to look at the long-time average of the flow. The experimental data were taken using a two-camera, particle image velocimetry (PIV) system. There were 750 data pairs taken (from which the velocities were computed) over typical time intervals of 375 seconds, representing very long-time averages of the flow variables.[5] The question is: What length of time is needed for the unsteady computations in order to obtain a long-time average with an acceptable error? FLUENT provides for the long time average of the Reynolds-averaged flow quantities (except Reynolds stresses).

Figures 9-11 plot the normalized l_2 norm of the long-time averaged streamwise (U) and transverse (V) velocity profiles at the outlet to the physical model with time for grids "a," "b," and "c." The normalized l_2 norm is computed based on:

$$l_2 = \left[\sum_{i=1}^{N}(s - s_o)^2\right]^{1/2} \Big/ \left[\sum_{i=1}^{N} s_o^2\right]^{1/2} \tag{1}$$

where s is the quantity in question, s_o is a reference value (based on the last profile computed) and N is the number of nodes in a profile. The difference should either be minimal or not changing very much.

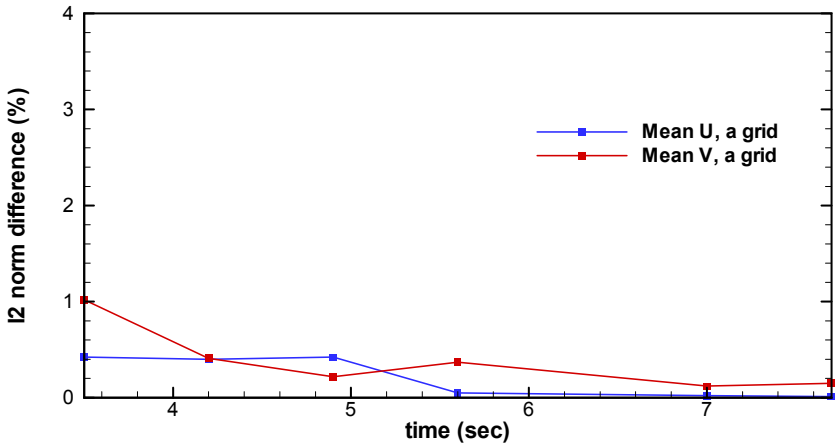

Figure 9. l_2 normalized differences for grid "a" for U and V. Ref. time = 8.575 sec.

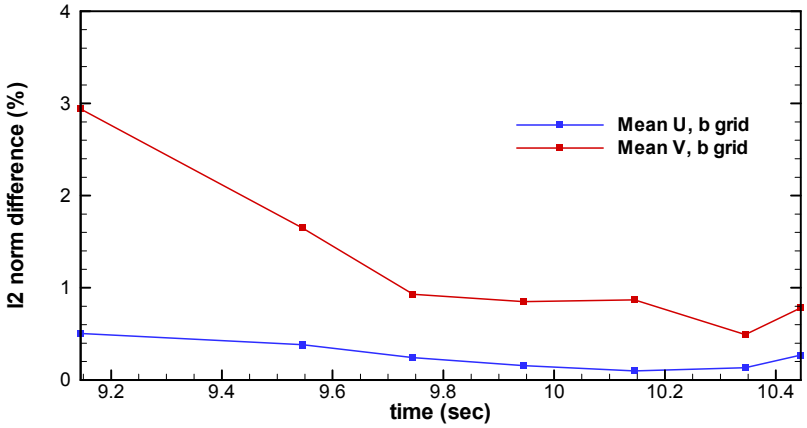

Figure 10. l_2 normalized differences for grid "b'' for U and V. Ref. time = 10.5451 sec.

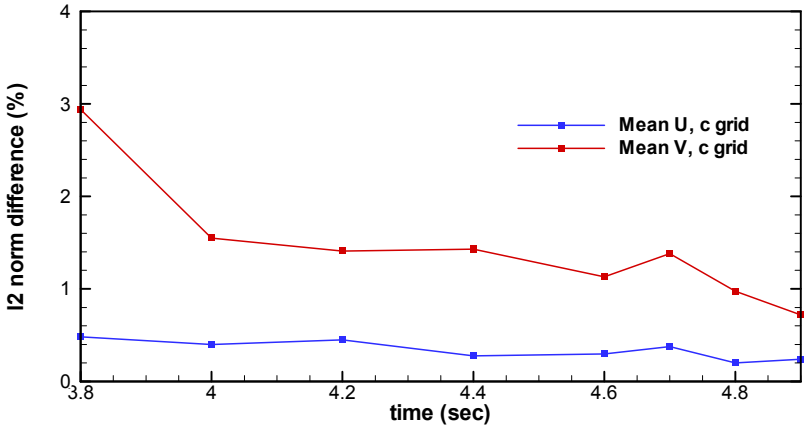

Figure 11. l_2 normalized differences for grid "c" for U and V. Ref. time = 5.0 sec.

Figures 12 and 13 illustrate the long-time averaged or mean velocity profiles for U and V at the CFD model outlet for the three grids. The results for the coarsest grid, "a", are visibly different from the other results. The mean U results for the "b" and "c"' grids appear very close. The results for mean V indicate that results on the finest two grids, "b" and "c"', are not quite symmetric. The asymmetric variations are greater than the variations caused by grid refinement. One can take the view that there may be some effect that has a relatively long time scale that has not yet been captured in the time scales of the present simulations, but that grid "b" is provisionally appropriate for further calculations.

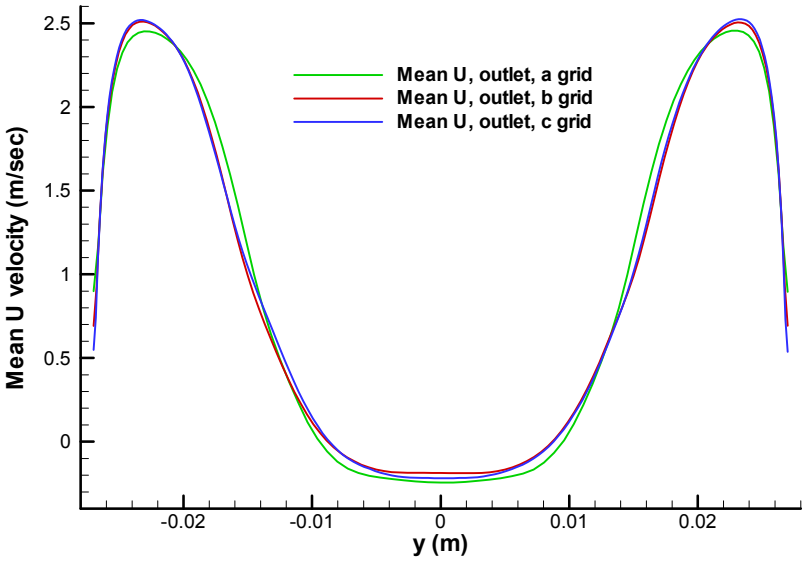

Figure 12. Comparison of the long-time averaged U velocity profiles at the outlet for grids "a," "b," and "c."

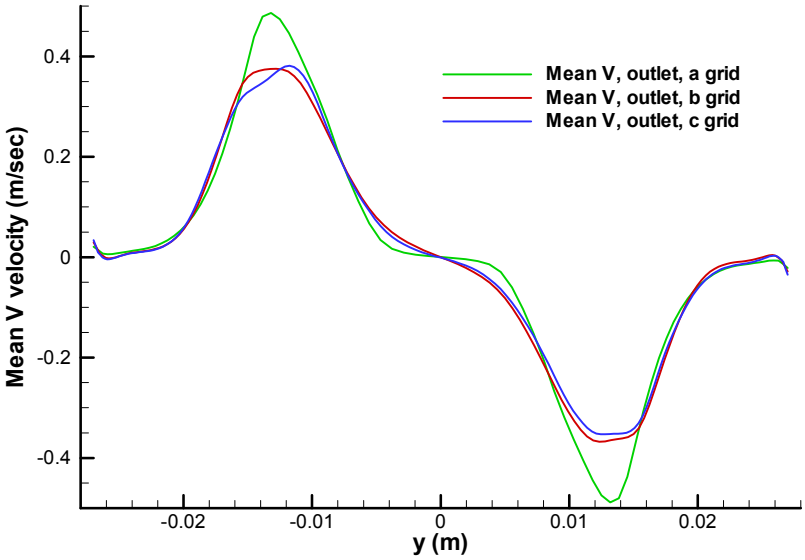

Figure 13. Comparison of the long-time averaged V velocity profiles at the outlet for grids "a," "b," and "c."

The profiles shown in Figures 12 and 13 (whose nodes are not coincident) can also be compared mathematically using an L_2 norm based on a finite-element-style integration over the domain of the profile. The L_2 norm is computed based on the formula:

$$L_2 = \frac{\left\{\int_\Omega \left[s(y,t) - s_o(y,t_o)\right]^2 dy\right\}^{1/2}}{\left\{\int_\Omega s_o^2(y,t_o)dy\right\}^{1/2}} \tag{2}$$

where Ω is the domain of the profile. Using Eqn. 2, with the finest grid "c" being used as the reference profile, the L_2 norm for profiles for the "a" and "b" grids are 6.1% and 2.1% for the U velocity and 22.2% and 5.7% for the V velocity.

With a provisional grid chosen, additional simulations can be made to compare velocity profiles for the two different outlet boundary conditions for the "inside-only" CFD models with the "inner+outer" CFD model. The inside geometry for all of these simulations is given in Figure 5.

Initial computations were made using the CFD model that includes the outer flow domain. Figure 14 illustrates the stream function [2] at a point in time of the flow. As can be seen, there is vortex-shedding occurring behind the thick walls of the physical model that interacts with the flow exiting from the model; this flow also contains shedding vortices. Based on this observation alone, one can conclude that, at least at the exit plane of the physical model, the flow simulations for the inside-only CFD models cannot be the same as those for the CFD model that includes the outer flow. Also, vortices are being shed behind every full and half cylinder.

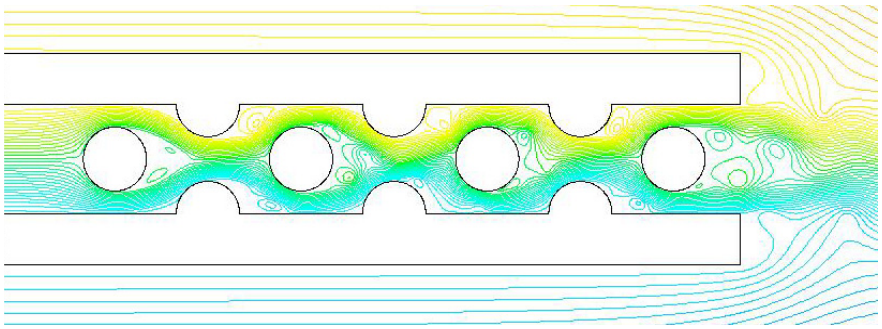

Figure 14. Stream function contours of the flow in the CFD model that includes the outer flow showing vortex-shedding behind the physical model in the MIR test loop.

Long-time calculations were made for the three CFD models, namely, the ”inside-only” models using the “pressure-outlet” and the “outflow” boundary conditions and the “inner+outer” model, all using $\Delta t = 7.5 \times 10^{-5}$ secs. To see if the simulations have been made for a sufficiently long time period, the l_2 norm of the outlet plane profiles at several points in time has been computed for each model as was done previously using Eqn. 1. Figures 15-17 plot the l_2 norm results as functions of time for the three cases.

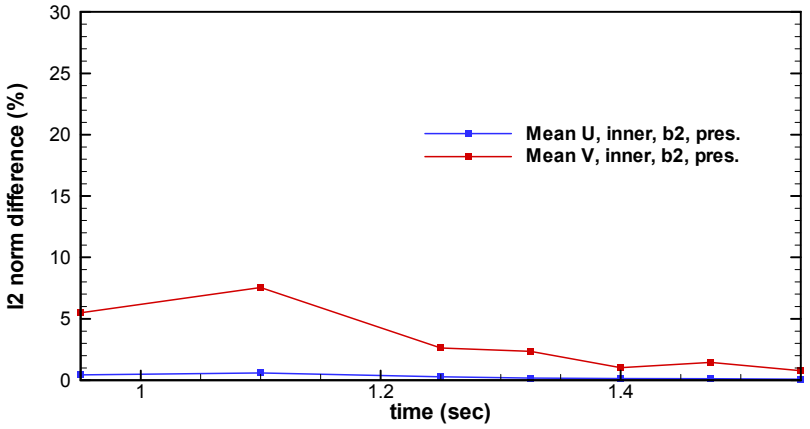

Figure 15. l_2 differences for the “inside-only” ”pressure-outlet” model. Ref. time = 1.5932 sec.

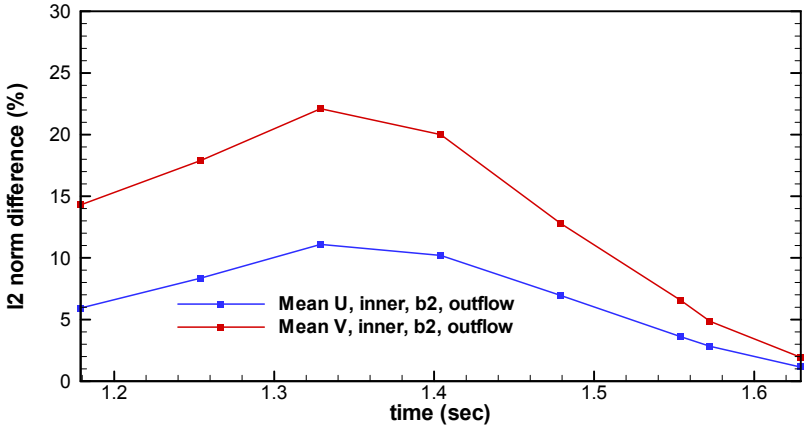

Figure 16. l_2 differences for the ”inside-only” “outflow” model. Ref. time = 1.6953 sec.

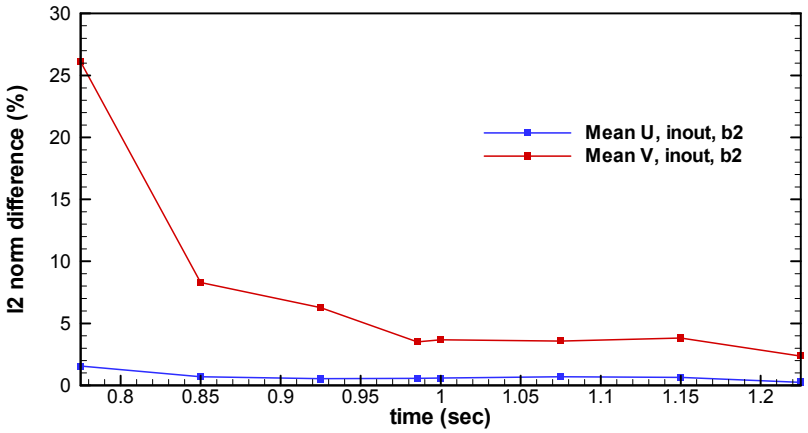

Figure 17. l_2 differences for the "inner+outer" model. Ref. time = 1.2909 sec.

The time profiles of the l_2 norms for the three cases appear to show adequate time for the long-time averages, though additional time could be added to ensure such.

Additional information can be obtained from plotting time signature data from points in the flow fields. Figure 18 illustrates the locations of points from which data are plotted. Figure 19 plots the long-time-averaged velocities U at points p3 and p4 and the Reynolds-averaged velocity u at point p5 for the "inner+outer" model. The mean velocities U at p3 and p4 appear to be stationary at this scale. The Reynolds-averaged velocity u at p5 exhibits at least two time scales of unsteadiness. The time scale of the smallest cycle ranges from 0.01 – 0.02 secs, while a pattern that repeats itself over 11 of the smaller cycles is apparent; the time scale of the larger pattern is 0.1634 secs. (1.0573 – 1.220725 sec.) Figure 20 plots the two mean velocities of Figure 19 at an expanded scale; it appears that the long-time averages are still changing in time. Additional simulations could be made for longer times to ensure that long-time averages are changing negligibly.

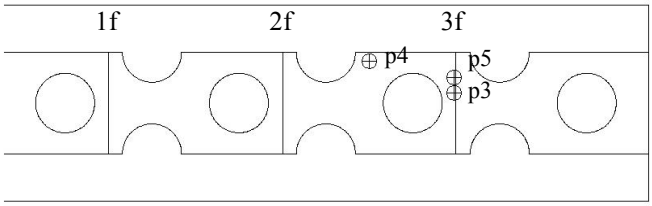

Figure 18. Locations of points and profile lines. Flow is left to right.

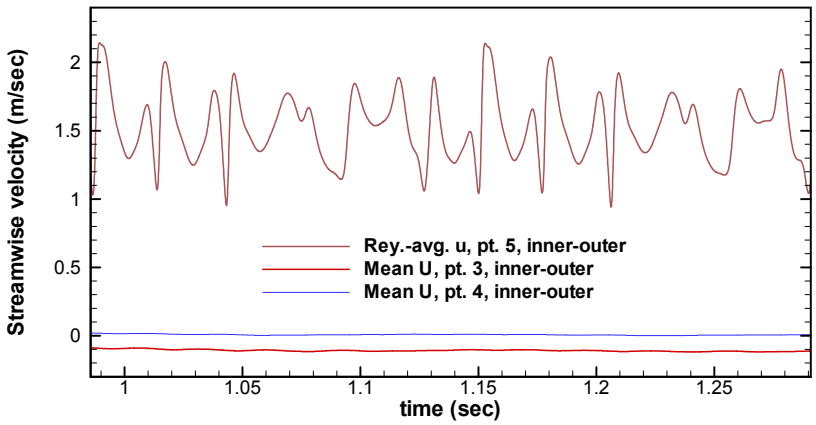

Figure 19. Long-time-averaged velocities U at points p3 and p4 and Reynolds-averaged velocity u at point p5; see Figure 18 for point locations.

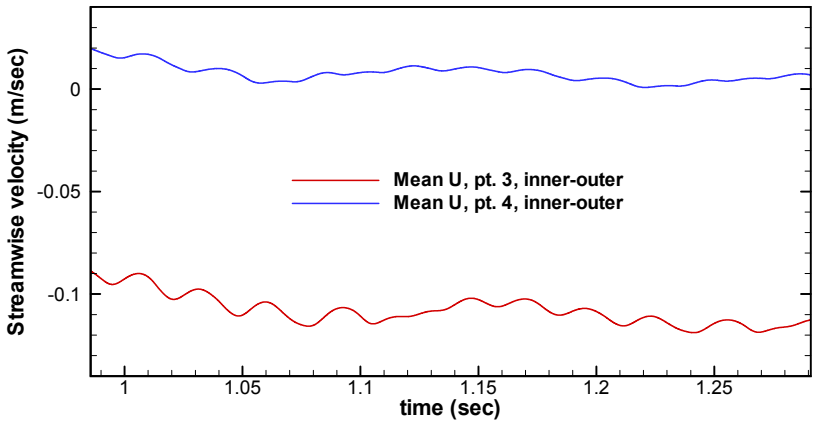

Figure 20. Same data from Figure 19 at points p3 and p4.

Figures 21 and 22 plot the Reynolds-averaged and long-time-averaged velocities at point p5 for the "inside-only" CFD models, using the "pressure-outlet" and "outflow" conditions, respectively. For the "pressure-outlet" case, a pattern of 11 cycles with overall length of 0.1638 secs (1.3898 – 1.5536 sec.) can be detected that matches the form of the longer time pattern of the "inner+outer" case of Figure 19 for the same p5. The pattern for the "outflow" case of Figure 22 does not resemble the patterns of the other two cases. The presence of multiple time scales is likely caused by the presence of multiple asynchronous vortex-shedding sites. Note that the time signatures of Figures 19, 21, and 22 are rather different from that of Figure 8, where there were fewer vortex-shedding sites (only two full and four half posts compared to four full posts and six half posts).

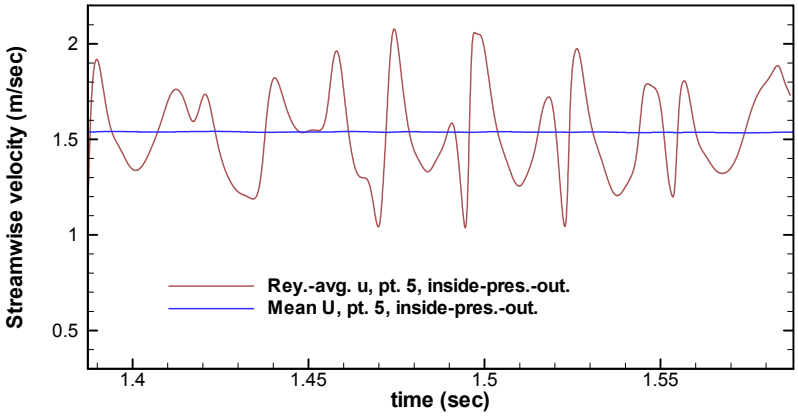

Figure 21. Long-time-averaged and Reynolds-averaged velocity at point p5 for "pressure-outlet" case.

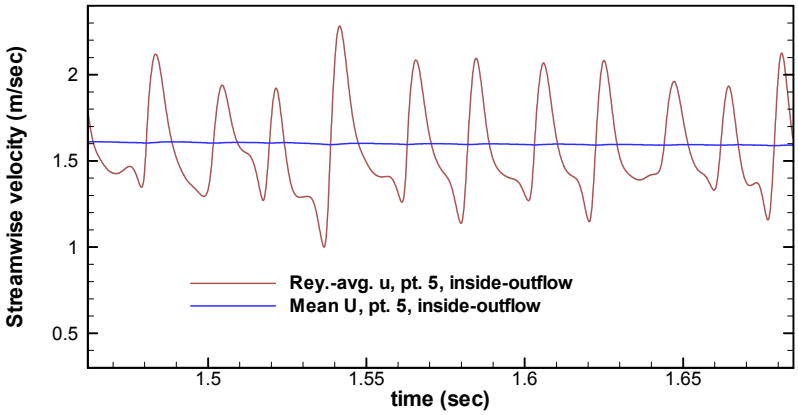

Figure 22. Long-time-averaged and Reynolds-averaged velocity at point p5 for "outflow" case.

Figure 23 plots the long-time-averaged velocity U at point p5 of Figure 22 for the "pressure-outlet" case at an expanded scale. Similar to the plots at points p3 and p4 of Figure 22, the long-time-average velocity appears to be still changing.

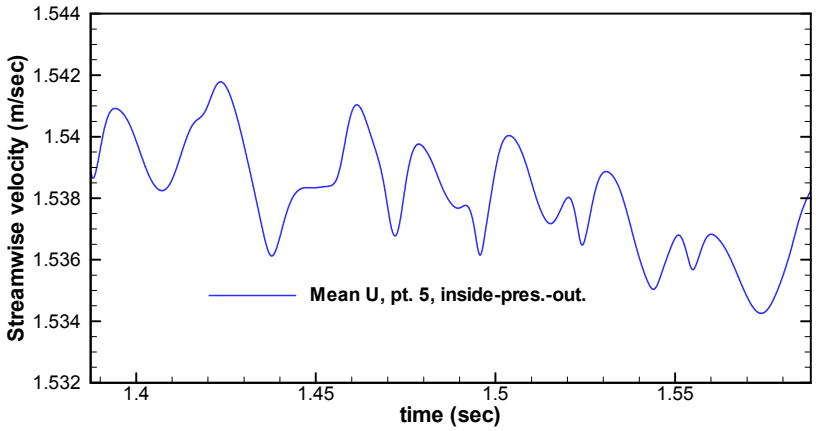

Figure 23. Long-time-averaged velocity U at point p5 from Figure 22.

Velocity profiles are now compared for the three CFD models. Figures 24-25 illustrate the long-time averaged U and V velocities at the physical model outlet, for the cases of the "inside-only" CFD models, using "pressure-outlet" and "outflow" boundary conditions, and for the "inner+outer" CFD model. Clearly, neither of the velocity profiles for the "inside-only" models matches results with the "inner+outer" model. However, results using the "pressure-outlet" boundary condition come much closer to the "inner+outer" results than do results using the "outflow" boundary condition. It should also be noted that there is continuous inflow at the outlet of the two "inside-only" models because of the recirculation associated with the shedding vortices around the final full post.

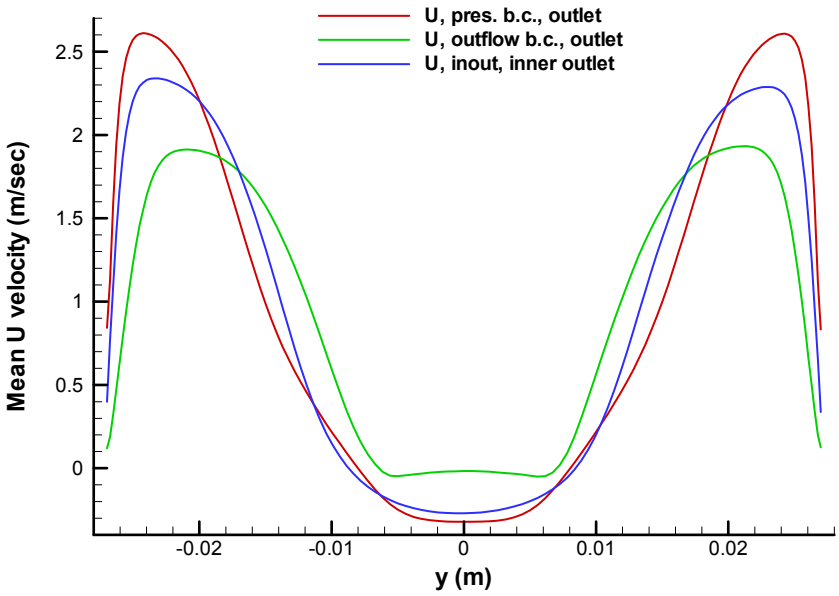

Figure 24. Profiles of long-time averaged U velocity at the physical model outlet for the "inside-only" CFD models, using "pressure-outlet" and "outflow" conditions, and for the "inner+outer" CFD model.

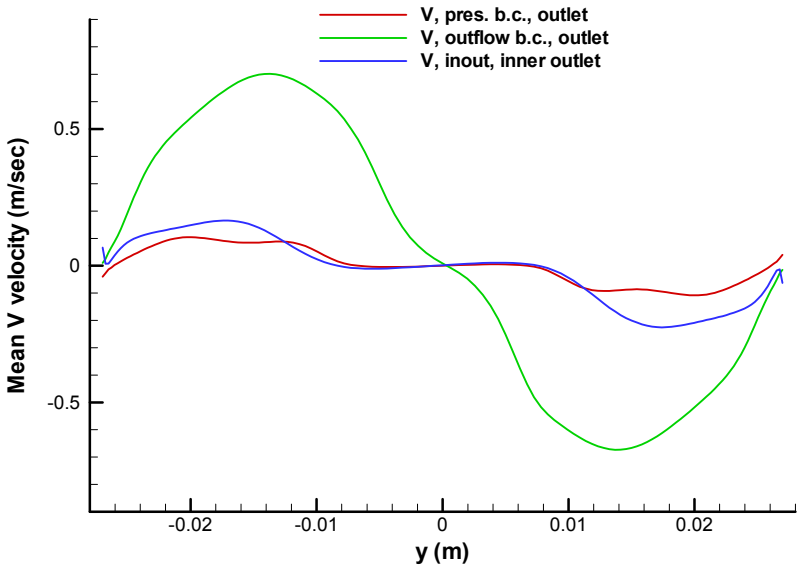

Figure 25. Same as Figure 24 for long-time averaged V velocity.

Velocity profiles at three additional locations are compared for the three CFD models to see the relative effects of the outlet boundary condition on upstream results and to see if either of the "inside-only" CFD model results compare well with those for the "inner+outer" CFD model.

Figures 26-31 illustrate long-time averaged U and V velocity profiles at axial locations 1f, 2f, and 3f. These locations are shown in Figure 18. The times of comparisons are at the reference times of Figures 15-17. Here, the profiles for the "inside-only" case using the "pressure-outlet" condition are remarkably close to those for the "inner+outer" case. Although these results are not considered validated, it is clear that results for the "inside-only" CFD model, using the "pressure-outlet" boundary condition, yield very similar results to the full "inner+outer" CFD model, at least from profile location "3f" and upstream. This means that the region on the outside of the physical model need not be included in the CFD model. The results for the "inside-only" case using the "outflow" condition are noticeably inferior to the "pressure-outlet" results, though they still show fair agreement with the "inner+outer" computations.

In addition to the long-time-averaged velocities, it is interesting to examine the results for the Reynolds shear stress. Figures 32-34 plot long-time-averaged Reynolds shear stress at locations 1f, 2f, and 3f for the three CFD models. The profiles for the "inside-only" "pressure-outlet" case are again remarkably close to those for the "inner+outer" model. And the results for the "inside-only" "outflow" case are still in fair agreement with the full CFD model.

The results for the "inside-only" "pressure-outlet" model are from simulation time 1.5932 secs, while those for the "inner+outer" case are from 1.2909 secs. This time difference is about two times the large 0.1638 sec patterns detected in Figures 19 and 21. With such a difference in the times of the two cases and in view of the remarkable agreement between their respective results upstream of the outlet, it appears that the long-time averages are not changing significantly and that extending the times of the calculations is not necessary.

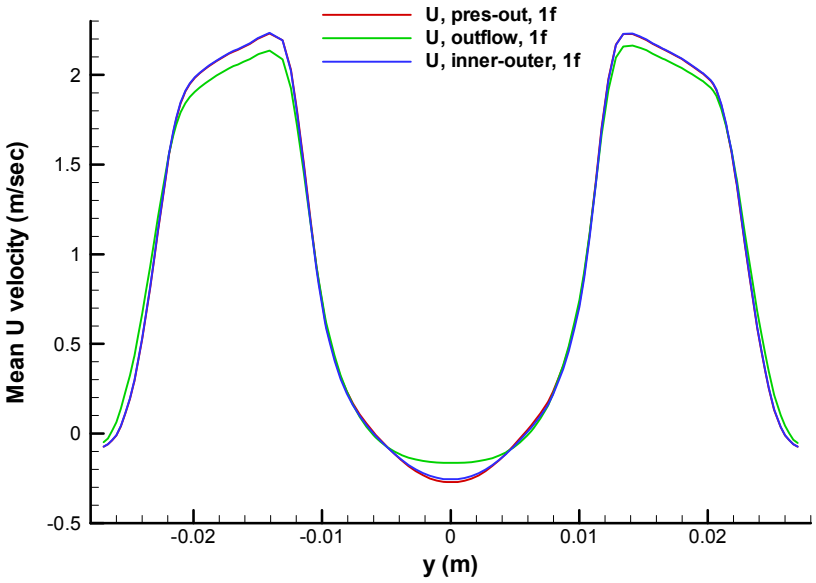

Figure 26. U velocity profiles at location 1f.

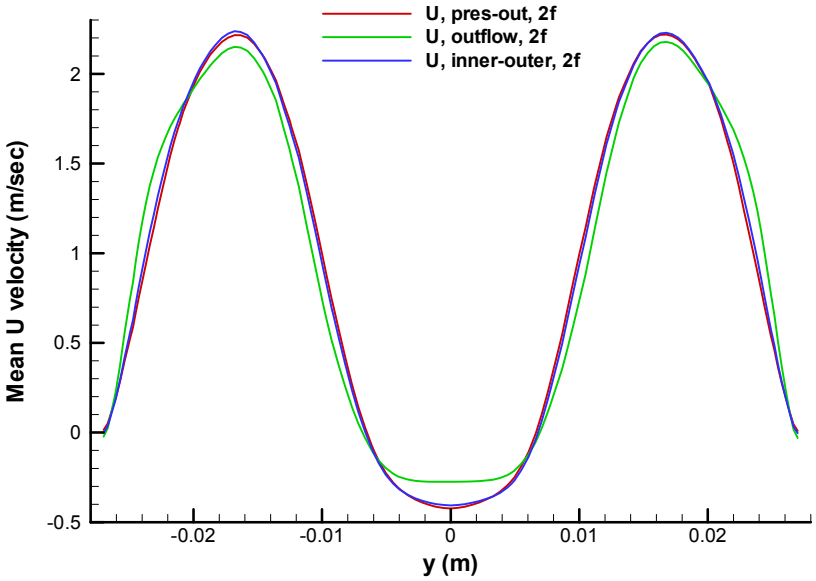

Figure 27. U velocity profiles at location 2f.

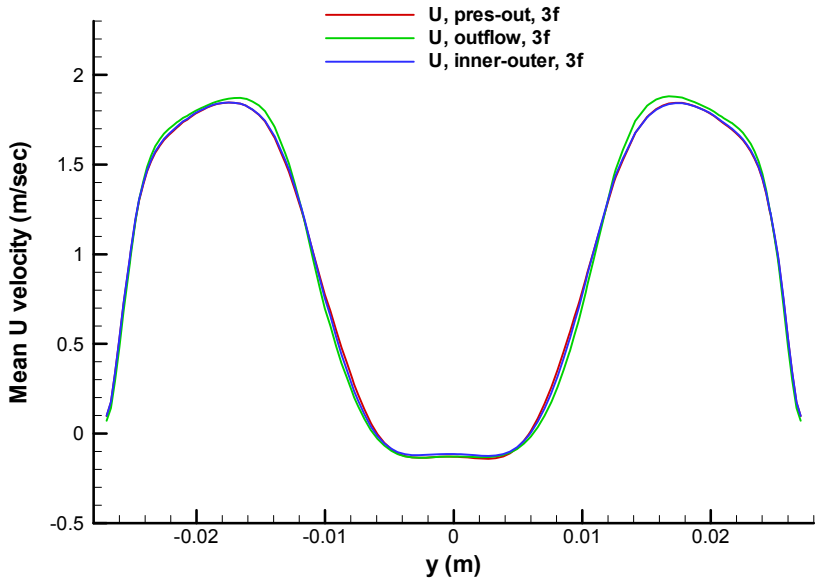

Figure 28. U velocity profiles at location 3f.

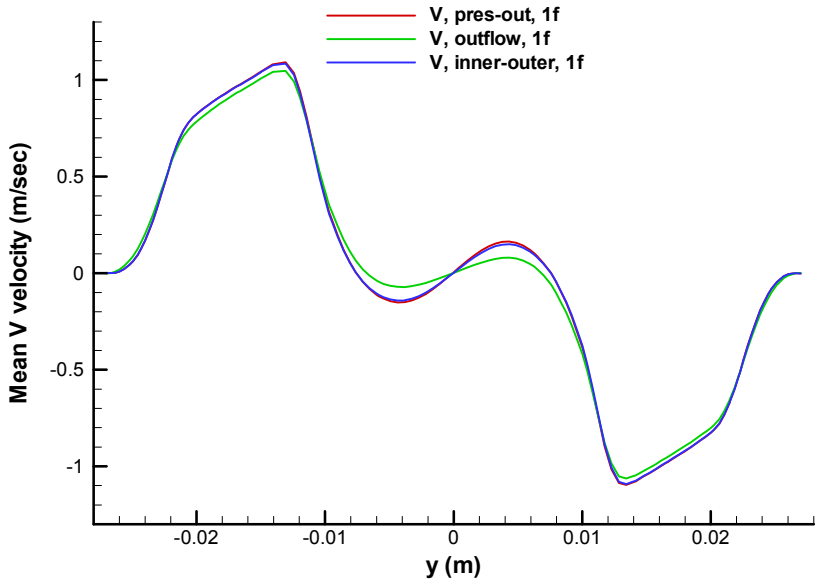

Figure 29. V velocity profiles at location 1f.

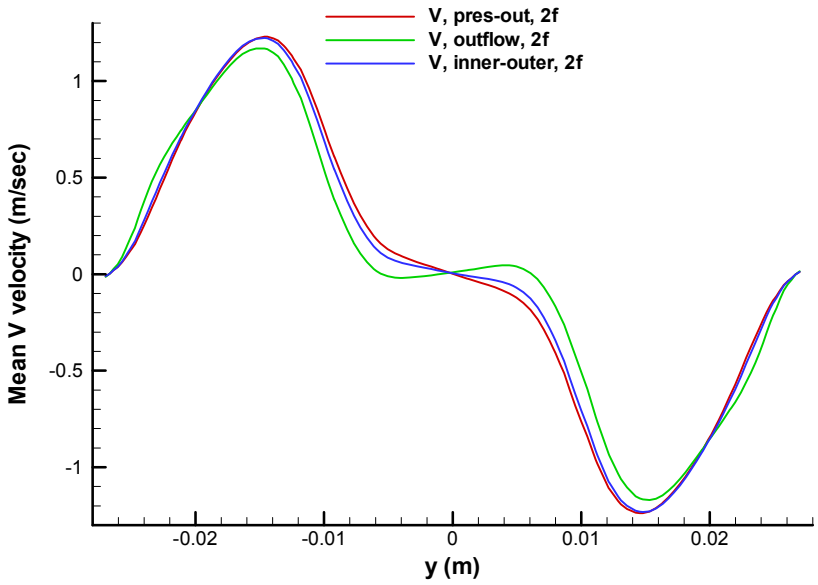

Figure 30. V velocity profiles at location 2f.

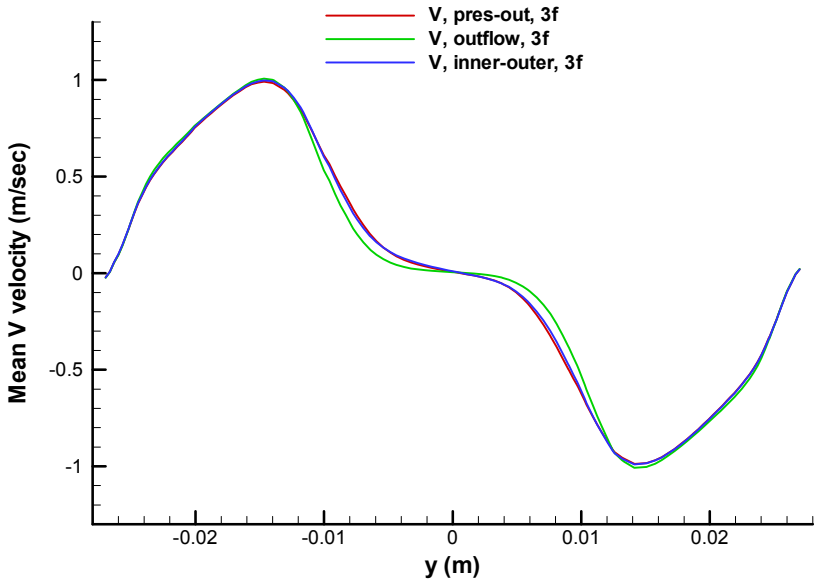

Figure 31. V velocity profiles at location 3f.

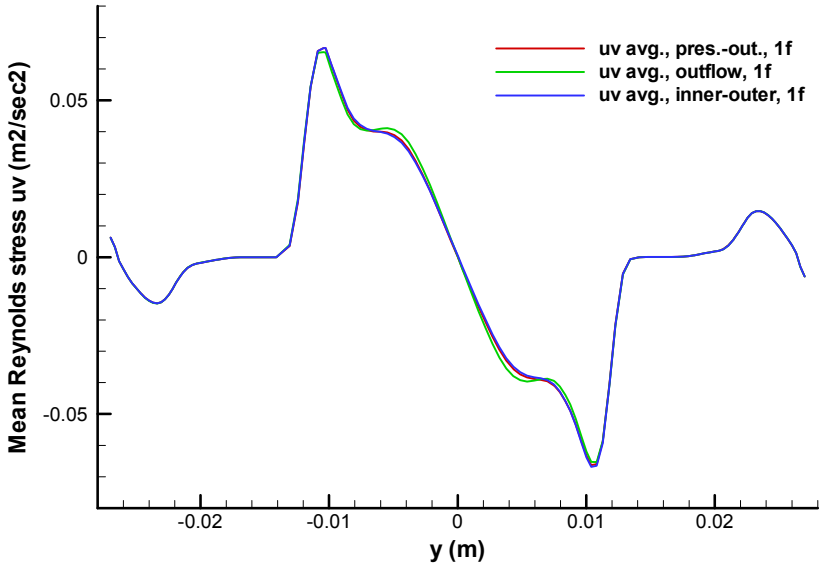

Figure 32. Long-time-averaged Reynolds stress $\overline{uv}$ at location 1f for the three CFD models.

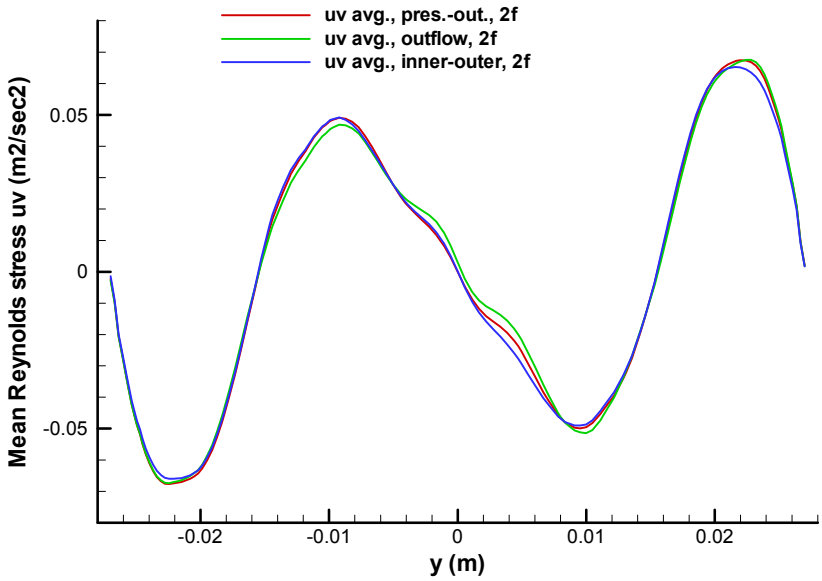

Figure 33. Long-time-averaged Reynolds stress $\overline{uv}$ at location 2f for the three CFD models.

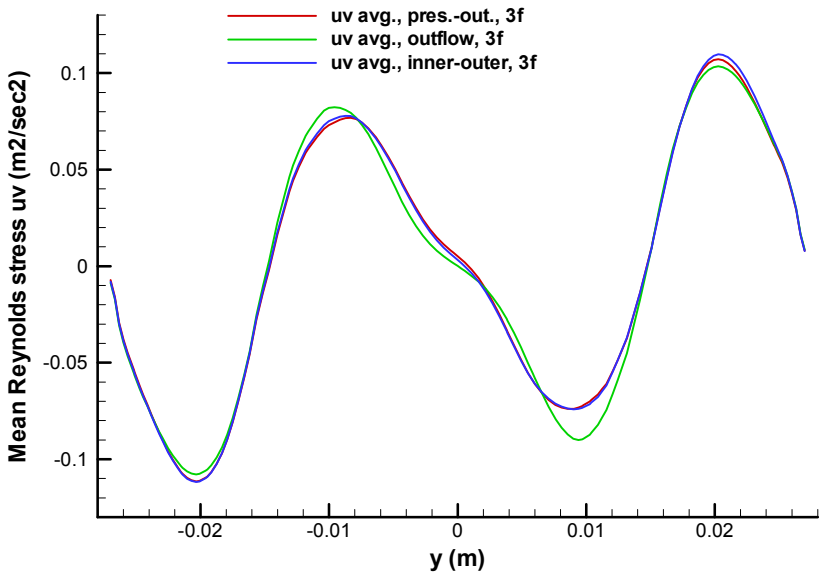

Figure 34. Long-time-averaged Reynolds stress $\overline{uv}$ at location 3f for the three CFD models.

In summary, investigations were made to help devise an analysis plan for the CFD analysis of the 3-D scaled model of a portion of a prismatic VHTR lower plenum. Employing 2-D CFD models of the scaled physical model wherein most of the interior of the model was replicated, it has been found that the inclusion of the outer flow around the model is not necessary to obtain adequate numerical representations of the flow field inside of the model, but upstream of the exit and not including the exit region. The "pressure-outlet" condition, available in the commercial CFD code FLUENT,[2] provides adequate simulations when compared to the case where the outer flow is included in the flow domain. The case where the "outflow" outlet boundary condition is used produces only fair agreement with the "inner+outer" calculations. The former condition applies a constant static pressure just beyond the exit plane of the outlet; the latter enforces constant derivatives for the velocities at the exit plane.

Furthermore, it was found that for the 2-D models, at least, the realizable k~ε model, using either the enhanced wall model or standard wall functions in FLUENT with a grid suitable for the enhanced wall model, does not predict vortex shedding. The Reynolds stress model (RSM), using standard wall functions, does provide for vortex shedding even without a "numerical kick."

3. RESULTS AND DISCUSSIONS FOR 3-D SIMULATIONS

3-D analyses of the Standard Problem geometry have been made using commercial CFD codes, including both steady and unsteady calculations. Steady calculations were made to compare results from several meshes and to investigate the steady results. Unsteady computations were made to investigate issues associated with simulating the actual flow, which is expected to be unsteady because of the presence of unsteady vortex-shedding. Three general-purpose, commercial, finite-volume-method CFD codes have been identified as likely candidates for use in the design and analysis of the NGNP:

- STAR-CD (version 4.06)[6]
- STAR-CCM+ (version 3.04)[Error! Reference source not found.]
- FLUENT (version 6.3)[2]

The first two are distributed by CD-adapco Group, which is headquarted in Melville, NY. The latter is distributed by Fluent Inc. (owned by ANSYS, Inc.), headquartered in Lebanon, NH. It is expected that additional general-purpose software packages and special-purpose codes will be included when the Standard Problem is opened to broader participation by the reactor design and analysis community as a standard benchmark problem.

As a first step in this preliminary benchmarking effort, a comprehensive set of tables of features of the three codes currently considered was developed. Features listed in the table include solvers, turbulence models, discretization methods, and additional physics models. Although cost of licensing has been discussed as an important factor in the selection of a CFD code or codes for use in the simulation of the NGNP, it is not included explicitly in the current table. Initial table entries for STAR-CD and + are shown in Appendix C. Inasmuch as FLUENT is limited in terms of number of parallel licenses available, it is not currently being applied for the 3-D simulations.

3.1 Steady 3-D Simulations

A CAD model describing the test section geometry was developed as a basis for the development of the computational meshes for the steady computations. The CAD model, shown in Figure 35a, currently includes the complete geometry of the lower plenum test section with four inlet jets entering the volume. The inlet feed lines are simplified as straight cylindrical tubes with sufficient length to provide a flow development length of 10 L/D. An initial graphics exchange specification (IGES)-formatted geometry description was exported from the CAD software, and a triangulated surface mesh was generated. The surface mesh uses triangles with a maximum length scale of 5 mm and a minimum length scale of 0.25 mm. In this mesh, a circle is required to be defined by a minimum of 36 cell edges and a minimum of three cells are required along any edge or between any two edges. The surface mesh, see Figure 35b, consists of 84,500 triangular surface cells.

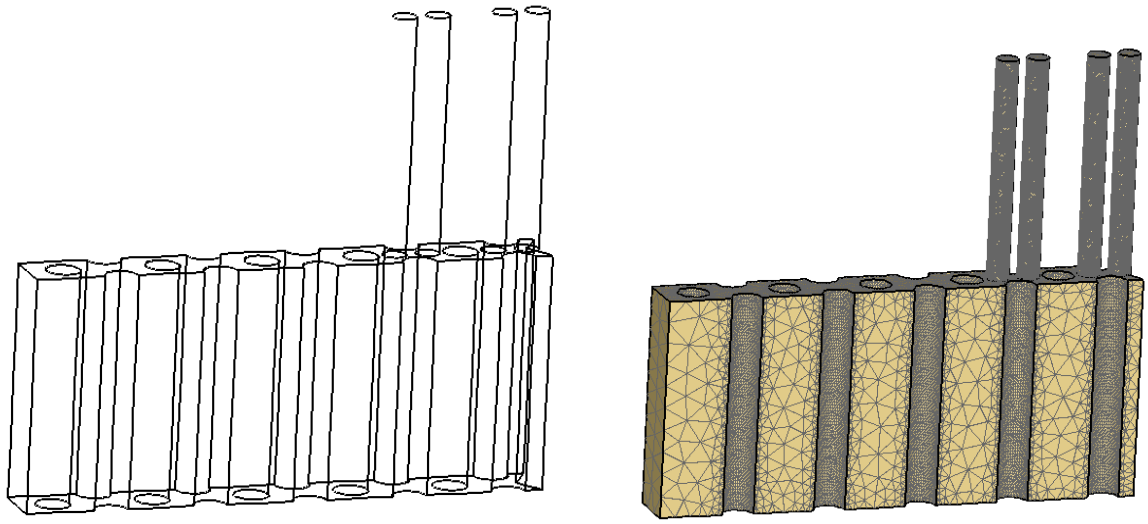

(a) (b)

Figure 35. (a) IGES format CAD representation of the geometry of the Standard Problem and (b) its surface mesh representation.

With the triangulated mesh as a starting point, an initial volumetric computational mesh was constructed using the automatic meshing tools of STAR-CCM+. The volumetric mesh is automatically generated by:

- Shrinking the surface mesh to create a sub-surface
- Generating a hexahedral mesh based on the maximum cell size specification that spans the domain of the model
- Locally refining the hexahedral mesh to the target cell size where surfaces pass through hexahedral elements
- Further refining locally to as small as the minimum cell size will allow to accommodate targets for number of cells on a circle or number of points in a gap
- Trimming away any cells or parts of cells that fall outside the sub-surface
- Extruding prismatic layers between the subsurface and the original surface.

A horizontal cross-section of a typical computational mesh resulting from this methodology is shown in Figure 36a. Local refinement in the near wall regions and, particularly near the cylindrical support columns, is easily seen in this view. A vertical cross-section is shown in Figure 36b. While the procedure can be simplified by eliminating steps 1 and 6, the more complex procedure has the benefit of moving the trimmed cells away from the wall surfaces and providing cells near the wall that have faces that are roughly orthogonal to the flow direction, providing better numerical stability and generally reducing the importance of higher order gradient terms near the wall. STAR-CCM+ meshes are exported to STAR-CD file formats for STAR-CD simulations.

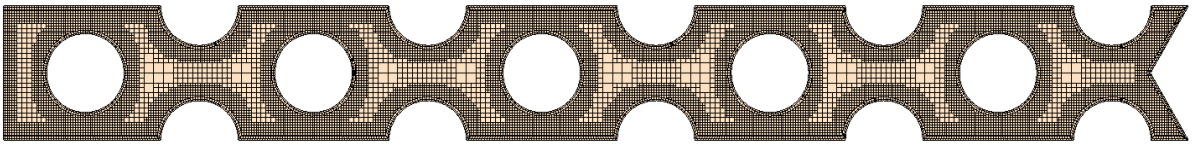

(a)

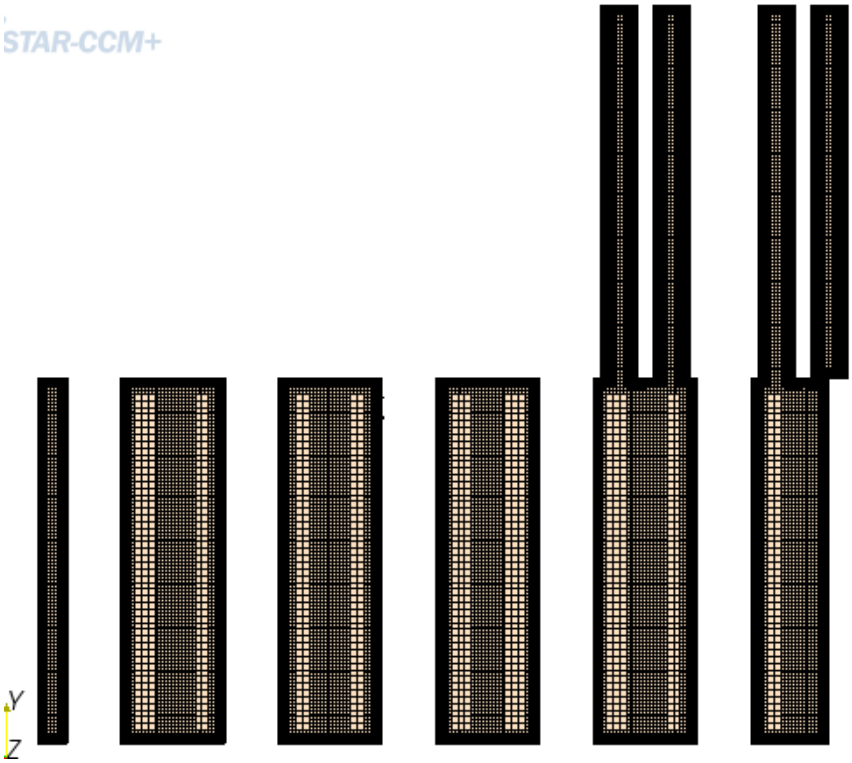

(b)

Figure 36. (a) Horizontal and (b) vertical cross-sections of the initial volumetric trimmed cell mesh developed for the Standard Problem geometry.

A mesh sensitivity study using seven unique computational meshes was completed using both STAR-CCM+ and, to a lesser extent, STAR-CD to aid in developing preliminary guidance on the meshing requirements for the 3-D Standard Problem. Initial mesh size scales were based on prior experience with the simulation of the tube bank validation case of Simonin and Barcuda.[8,9] The standard two-layer-high Reynolds number k~ε model was used for all meshes included in these sensitivity studies.

The mesh size and structure characteristics are summarized in Table 1. Meshes A, B, and C, are trimmed cell meshes with no extrusion layer near the surface, and have three different mesh densities, with mesh A using nominal mesh size characteristics, mesh B providing a significantly coarser mesh representation of the geometry, and mesh C providing a significantly more refined mesh representation. Meshes D, E, and F are also trimmed cell meshes, but incorporate a prismatic extrusion layer of uniform thickness along all of the surfaces of the model, as shown in Figure 37. Mesh D is again based on the nominal mesh characteristics from the tube bank simulations, and mesh E provides a significantly coarsened mesh. In mesh F, the bulk cell-size characteristics of mesh D are maintained, but the number of layers in the extrusion layer is reduced from 3 to 2.

Mesh G is a trimmed cell mesh with mesh characteristics similar to those of Mesh D, but a specially tailored extrusion layer, which is designed to provide a more uniform distribution of the dimensionless boundary layer thickness parameter, y^+, throughout the model. Since the value of y^+ generally decreases as the flow moves from inlet to outlet, a tailored distribution was defined by assigning a unique scale factor to each surface in the model (ceiling, floor, each half post, each full post, each inlet tube and each side wall section). The scale factor determines the relative distribution of thickness of the three layers within the extrusion layer. The resulting near wall cell thickness distribution reduces the ratio of the maximum to minimum y^+ values from approximately 80 to approximately 4. An advantage of this approach is that the global average value of the y^+ parameter can be controlled by the global value of the extrusion layer thickness while the distribution of the local value of y^+ is controlled by the surface-based distribution of the scale ratio.

Table 1. Summary of mesh characteristics for the several meshes used in the 3-D mesh sensitivity study.

	Cell Count	Max Cell Size	Target Wall Cell Size	Minimum Cell Size	Prismatic Layer Thickness	Number of Prismatic Layers
A	3006544	10	1	0.25	N/A	N/A
B	575372	10	2	0.5	N/A	N/A
C	14855308	1	0.5	0.25	N/A	N/A
D	3914452	10	1	0.25	2.75	3
E	3832345	10	1	0.25	1.45	2
F	775587	10	2	0.5	2.75	3
G	3912156	10	1	0.25	varies	3

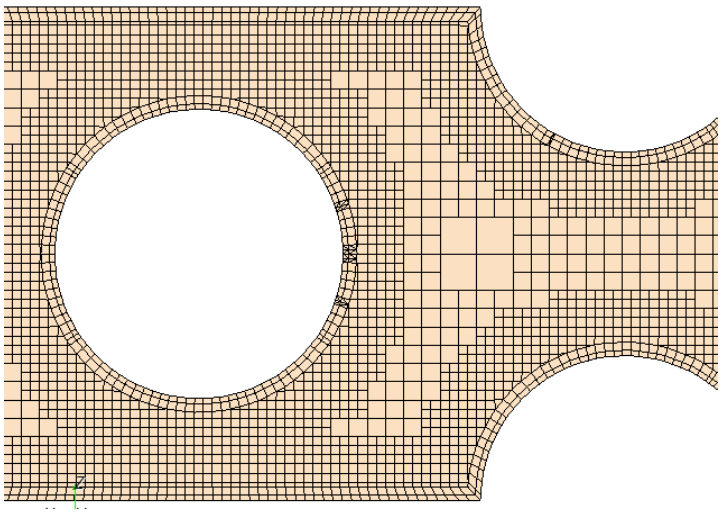

Figure 37. Close-up view of the mesh structure around the cylindrical support columns showing the location of the trimmed cells and the structure of the prismatic extrusion layer.

In all models considered in both STAR-CCM+ and STAR-CD, the flow inlet is treated as a constant velocity mass flux inlet plane and the outlet is treated as a constant pressure outlet plane. The inlet region is extended away from the test section to allow space for the development of turbulent flow in the four inlet pipes. As part of these studies, the effect of the outlet condition was evaluated by extruding a similar outlet extension to move the outlet condition away from the region of interest. In these studies, only the high Reynolds number experiment has been considered. In this experiment, the first, partially-blocked jet

has an average inlet velocity of 7.922 m/s and a Reynolds number of 4312. The second, third, and fourth jet have matched average velocities of 7.918 m/s and Reynolds numbers of 12393. The outlet pressure boundary is set to an arbitrary pressure of 0 Pa, so that predicted pressures can be read directly as differential pressures. In reality, the outlet flow of the test section expands and mixes with the bulk flow of the MIR facility, resulting in an unknown 2-D pressure distribution across the test section outlet. Assuming that the average temperature of the MIR facility's mineral oil working fluid is 23.4°C, the density is calculated to be 831.1 kg/m^3 and the dynamic viscosity is 0.011685 kg/m-sec.

In this initial series of simulations, only steady-state simulations have been considered. In STAR-CCM+ simulations, the default segregated flow solver is applied. The default solver uses the SIMPLE algorithm with Rhie-Chow interpolation for pressure-velocity coupling and algebraic multi-grid preconditioning. A 2nd-order central differencing scheme was applied to all cases. In STAR-CD simulations, the segregated SIMPLE pressure predictor-corrector algorithm, conjugate gradient solver, and 2nd-order monotone advection and reconstruction (MARS) differencing scheme were employed. For both STAR-CCM+ and STAR-CD, the reduction of the equation residuals by four orders of magnitude, or, in other words, reducing the normalized residuals below 10^{-4}, is recommended. However, additional convergence (or lack of convergence) indicators must be considered, such as large oscillations in the residuals as they cross the pre-set threshold or significant fluctuations in the number of outlet boundary cells exhibiting reverse flow.

Simulations were initiated for each of the meshes, using STAR-CCM+ and for a limited subset of meshes using STAR-CD (meshes, A, B, D, and F). In all cases, well-converged solutions were unattainable. The residuals do approach the 10^{-4} threshold in some cases, but advancing to these residual levels requires very small, under-relaxation factors and very tight, inner iteration convergence tolerances, on the order of 10^{-7} for all equations. Even with these very tight criteria, significant fluctuations appear in many of the residuals, and there are a significant number of cells with reversed flow reported on the outlet boundary.

The minimum residual value achieved for the largest of the equation residuals is shown for simulations using both STAR-CCM+ and STAR-CD in Table 2. In all STAR-CCM+ cases, the largest of the equation residuals occurs for the pressure (or continuity) equation. In all STAR-CD cases, the largest residuals occur in the turbulent kinetic energy equation.

Table 2. Summary of convergence characteristics from the mesh sensitivity study completed for 3-D simulations of the MIR lower plenum experiments.

	Cell Count	Max Residual Star-CCM+	Max Residual Star-CD
A	3006544	7.46E-04	1.78E-04
B	575372	1.16E-04	1.78E-04
C	14855308	3.15E-04	N/A
D	3914452	3.91E-02	3.20E-04
E	3832345	1.00E-01	N/A
F	775587	diverged	1.87E-03
G	3912156	6.51E-04	N/A

In STAR-CCM+, iteration times are long, requiring 2-3 minutes per iteration for coarser meshes. The coarse mesh problems are distributed to 10 CPUs of a parallel cluster computing platform, based on prior parallel scalability experience with the code and the particular cluster computing platform. Finer meshes running on 30-60 processors of the same machine often require 30 minutes or more per iteration. In the

extreme cases, CPU use falls to less than 1% and network traffic is extremely high. These results indicate that significantly more data is being exchanged between nodes than would normally be expected for a domain decomposition of this type. Iteration times are much shorter and CPU usage is much improved when the conjugate gradient solver of STAR-CD is used. The results of the mesh sensitivity study would indicate that the meshes with an extrusion layer at the walls—meshes D, E, and F—do not allow a solution with a sufficiently tight convergence tolerance. However, mesh G, with an adjustable extrusion layer, does compete well with A, B, and C meshes, though the tolerance is still too loose.

Further investigation of the stability of the steady-state solution has shown that the steady-state simulations produce three dramatically different flow field predictions. It is not uncommon for true steady-state simulations of the Navier-Stokes equations to predict two or more modes of flow behavior when applied to problems that include inherent pseudo-periodic unsteadiness due to flow mechanisms such as vortex shedding. The three solutions are shown in Figures 38-40. In the first solution, the first two inlet jets penetrate all the way to the bottom of the test section, and multiple large recirculation zones appear in the solution. In the second solution, the two jets rapidly diffuse as they enter the test section, but no large recirculation zone forms. In this case, significantly more small-scale turbulence, which is modeled by the turbulence model, is introduced to the flow field. In the third solution, the jets penetrate further into the test section than in the second case, but turn toward the outlet immediately after entering the test section. The first case is the dominant solution in the STAR-CCM+ simulations and the third case is the dominant solution in the STAR-CD simulations. The second solution is observed with both solvers.

Since neither extensive flow visualization data nor time-resolved PIV data is available to confirm that any of the configurations dominates, in reality, it is conceivable that all these solutions may occur at different times in an unsteady scenario. Although the second solution seems much less likely to be persistent in the system, the result is at least plausible if only in that it exhibits no more numerical instability than the others and does not violate any physical laws or limits. It is assumed that the oscillatory nature of the solution provides a mechanism for switching between these states.

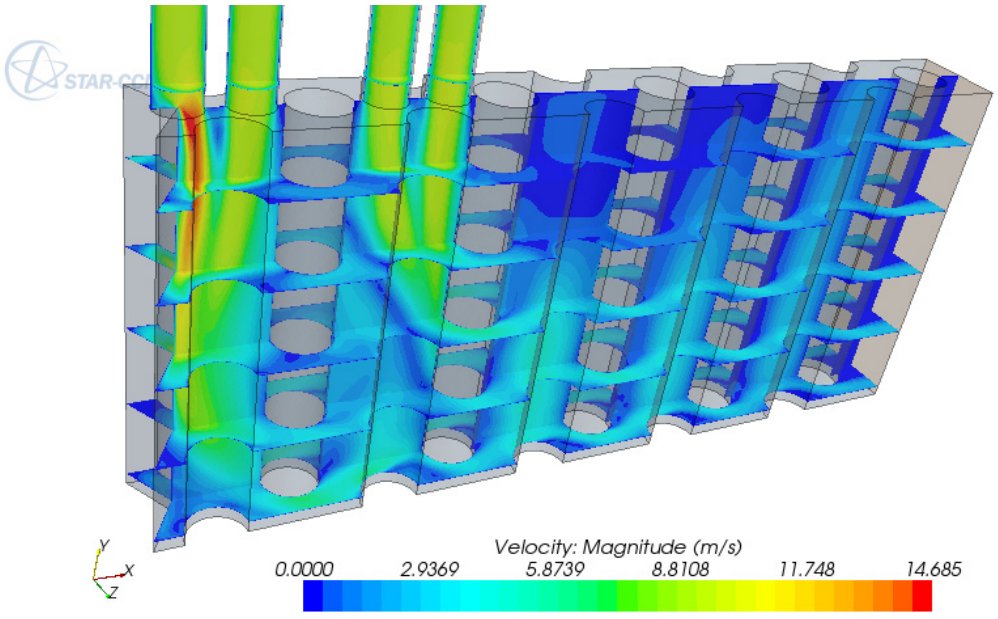

Figure 38. First observed solution in fully 3-D simulations of the MIR lower plenum experiments. Flow velocity magnitude is shown on the symmetry plane of the test section as well as five horizontal plane sections within the test section. Note that a large recirculation zone forms between the 2nd and 3rd jets and a second large recirculation zone forms along the surface of the upper boundary downstream of the 4th jet.

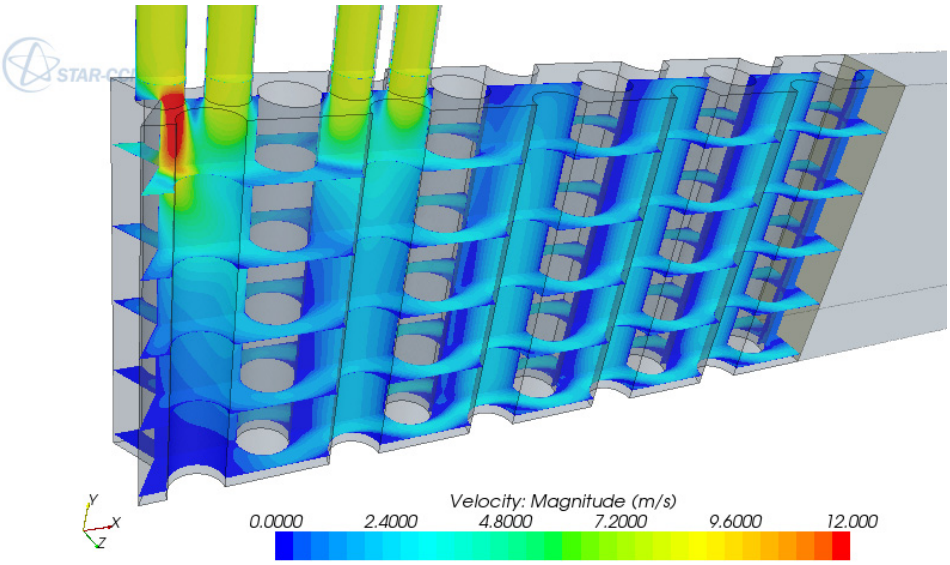

Figure 39. Second observed solution in fully 3-D simulations of the MIR lower plenum experiments. Flow velocity magnitude is shown on the symmetry plane of the test section as well as five horizontal plane sections within the test section. Note that the jets diffuse shortly after entering the test section and that no large recirculation zone forms in this case.

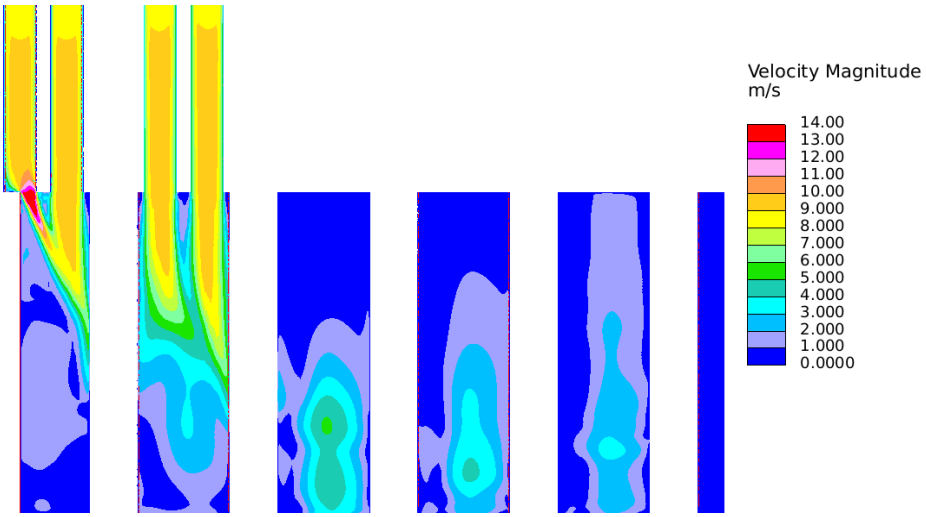

Figure 40. Third observed solution in fully 3-D simulations of the MIR lower plenum experiments. Flow velocity magnitude is shown on the symmetry plane of the test section. Note that the jets penetrate further into the test section than in the second observed solution but quickly turn toward the outlet, forming a large recirculation zone in the region below the first and second inlet.

In order to confirm that the observed behavior is not tied directly to the flow reversal at the outlet, two additional meshes were constructed which include long extrusion regions of different lengths from the original outlet face. This serves to isolate the test section from the potential instability associated with the outlet condition. Revised mesh characteristics are shown in Table 3, and the geometry of mesh H is shown in Figure 41. Somewhat surprisingly, the addition of the extruded outlet does not improve the convergence and the simulation actually stagnates with much higher average and minimum residual values. The number of outlet faces reporting reversed flow is reduced to single digits, however.

In order to confirm that the oscillatory behavior is not simply a function of the choice of turbulence model, the realizable two-layer formulation of the k-ε model was applied to the mesh with the shorter extended outlet region. No significant improvements in convergence characteristics or changes in the velocity field solution were observed. The conclusion that there is little change in the flow field compared to flow in the original geometry due to the added sections accords with the conclusion obtained from the development of the analysis plan that the presence or absence of the outer region flow only affects the region of the flow just near the exit to the physical model.

In conclusion, it appears that no steady-state solution can be reached because this geometry does not have one; rather, the flow should be unsteady because of the presence of shedding vortices behind the half and full posts.

Table 3. Mesh and convergence characteristics for computational meshes with an extruded outlet region.

	Cell Count	Max Cell Size	Target Wall Cell Size	Minimum Cell Size	Extrusion Length (m)	Max Residual
A	3006544	10	1	0.25	N/A	7.46E-04
H	3302194	10	1	0.25	0.3	5.27E-03
I	4189144	10	1	0.25	1.0	4.56E-03

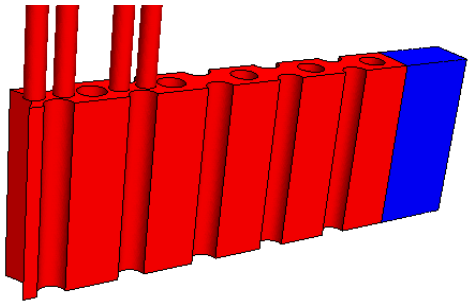

Figure 41. Geometry of the Standard Problem test section with extruded outlet extension to reduce influence of the outlet condition on flow field predictions.

Unsteady 3-D Simulations

The CFD model developed for the unsteady 3-D numerical simulations was informed by results obtained during the development of the analysis plan. The analysis plan addressed the issues of extent of the domain that needs to be included in the CFD model, grid convergence, time-step size, and boundary condition assignment, particularly at the outlet to the scaled model.

The initial grid built for the 3-D model is based on the grid study performed above, where the "b" grid was deemed to be fine enough for grid-independence. A similar grid was constructed using the meshing software GAMBIT, bundled with FLUENT[2]. The inlet ports were added and gridded the same or finer than the 2-D grid. The 2-D grid was then extruded upwards to construct the inlet ports and downwards to obtain the rest of the model geometry; the outer region outside of the model was not included, based on the conclusions obtained during the development of the analysis plan. The mesh cells in the 3-D grid are hexahedral. The number of cells allocated in the third dimension is 15 for the inlet jets and 125 in the body of the model. The physical model on which the CFD model was based has an overall length of 485.42 mm, a width of 53.98 mm, and a height of 217.50 mm (see Appendix A). The first two inlet jet ports have a height of 9.62 mm and the second two a height of 9.79 mm above the plane of the

inlet. The plane of the inlet contains the origin of the coordinate system. The vertical direction (z) is zero at the inlet plane, positive upwards. The streamwise direction (x) is actually 558.80 mm upstream of the outlet. The transverse direction (y) is zero at the symmetry plane that divides the model in half vertically. Figure 42 illustrates the geometry of the 3-D mesh and the origin of the coordinate system (in the upper left corner). Figure 43 illustrates a closeup of the mesh at the inlet plane near where the inlet jets are located. The 3-D mesh contains approximately 14 million cells.

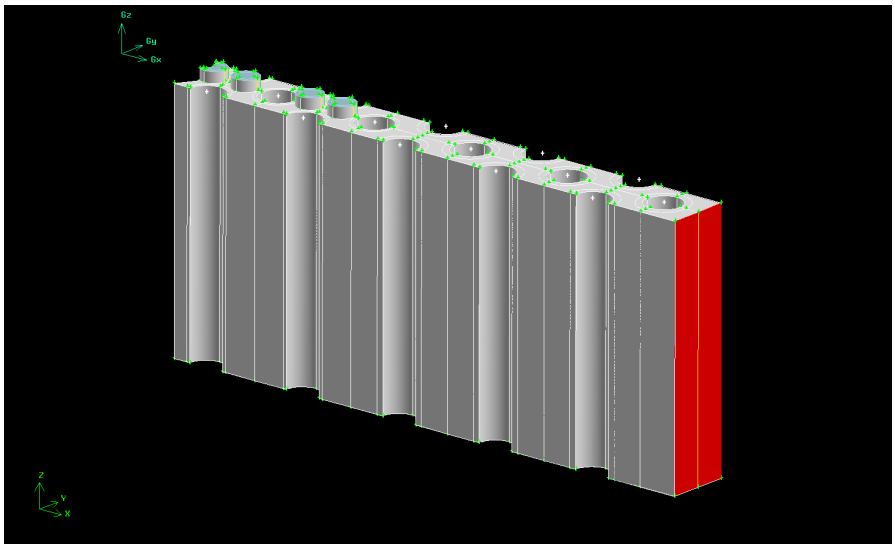

Figure 42. Geometry of the extruded 3-D mesh for the Standard Problem. The boundaries of the model are shown as gray for walls, green for the inlet boundaries, and red for the outlet.

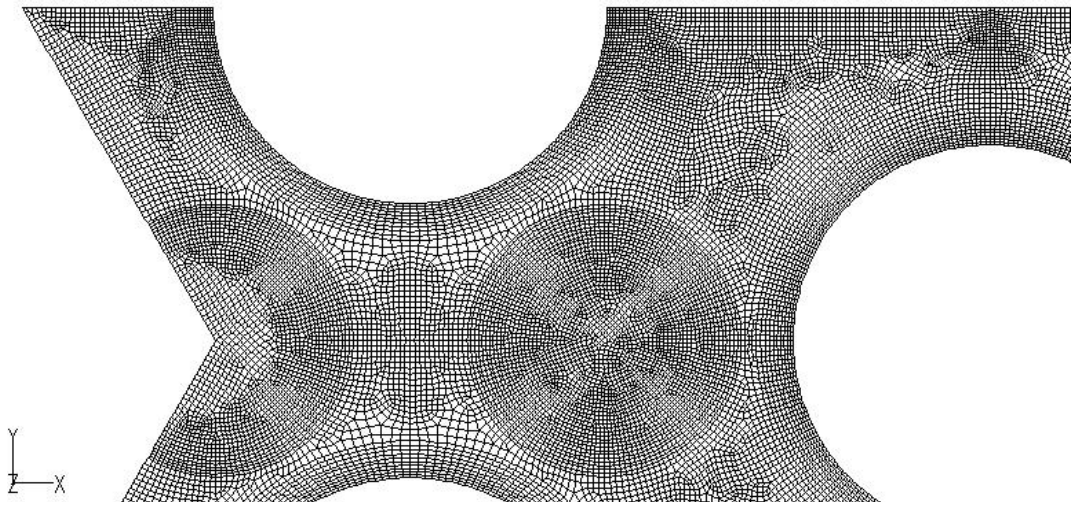

Figure 43. Closeup of 3-D mesh (14 million cells) showing local gridding details.

The commercial CFD code STAR-CCM+[7] was used for the 3-D simulations, inasmuch as a large number of parallel licenses are available at the INL for its use (in contrast to FLUENT, for which there are only 5 parallel licenses available). The initial simulations using the 14 million-cell mesh used a time step of 7.5×10^{-5} sec. to avoid the numerical event shown above in Figure 8 for the 2-D simulations.

STAR-CCM+ only has the pressure-outlet boundary condition. The Reynolds stress model (RSM), using the linear pressure-strain option, was used, which is similar to the RSM in FLUENT. The unsteady problem was initiated by first running a steady-state problem to a point where it would converge no further, and then starting the unsteady run.

The residuals in STAR-CCM+ are computed differently than for FLUENT. It was found by running a simple Poiseuille flow problem, which has an analytical solution, that a tolerance of about 1×10^{-4} for the residuals for the continuity and velocity components is adequate to obtain convergence. Hence, this tolerance is the target for the inner iterations made at each time step; it was found that 20 inner iterations provided about this level of convergence.

It has been found that with so many cells in the 3D mesh, parallel processing must be employed. However, it is usually the case that doubling the number of processors does not necessarily halve the time it takes to make a particular computation. Several runs were made using various numbers of processors and computing the speedup for each doubling of the number of processors. Figure 44 illustrates the results of this study. The speedup is based on the time required for the smallest number of processors used (32) and uses the same time step and number of inner iterations for each case.

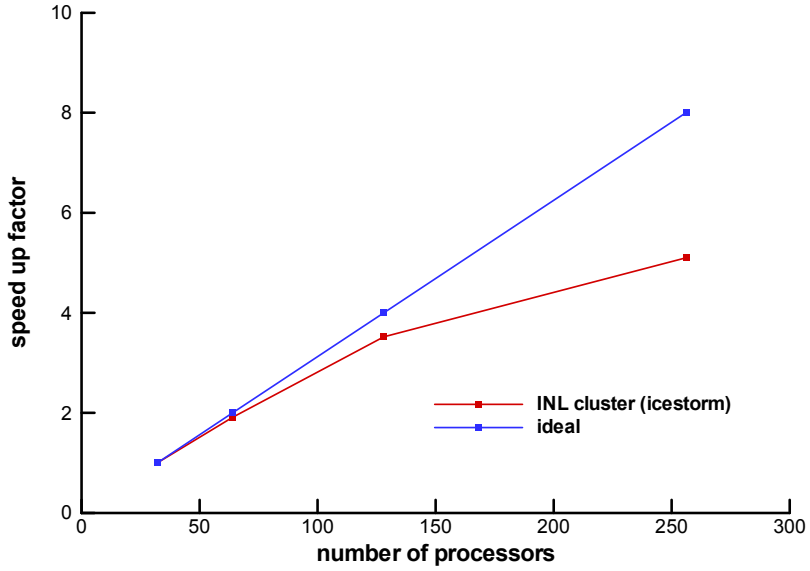

Figure 44. Speedup in the computations based on the baseline of 32 processors for the 14 million cell mesh.

A long-time computation of about 1.2 seconds net flow time was made using the 14 million cell mesh. (The computation starts at about 0.4 sec. because the solution was once cleared, but not reset to time zero.) Major features of the 3-D flow can be seen by computing a streamline field for a point in time for the flow. Figure 45 illustrates a streamline field for the flow at 1.27 seconds flow time. The streamlines are colored by velocity magnitude. As shown, the highest velocity magnitude occurs at the four inlet jet positions, where the streamlines originate. The flow generally moves downward and later upwards and towards the outlet to the left. Large recirculation regions can be seen below the rightmost jet and between the second and third jets. There is also a region of recirculation just to the left of the fourth jet. This region is also a region of relatively slow flow. While it is not clear whether there will be shedding vortices for the posts in the region near the inlet jets, there probably should be downstream where the flow moves generally to the right and mostly horizontally.

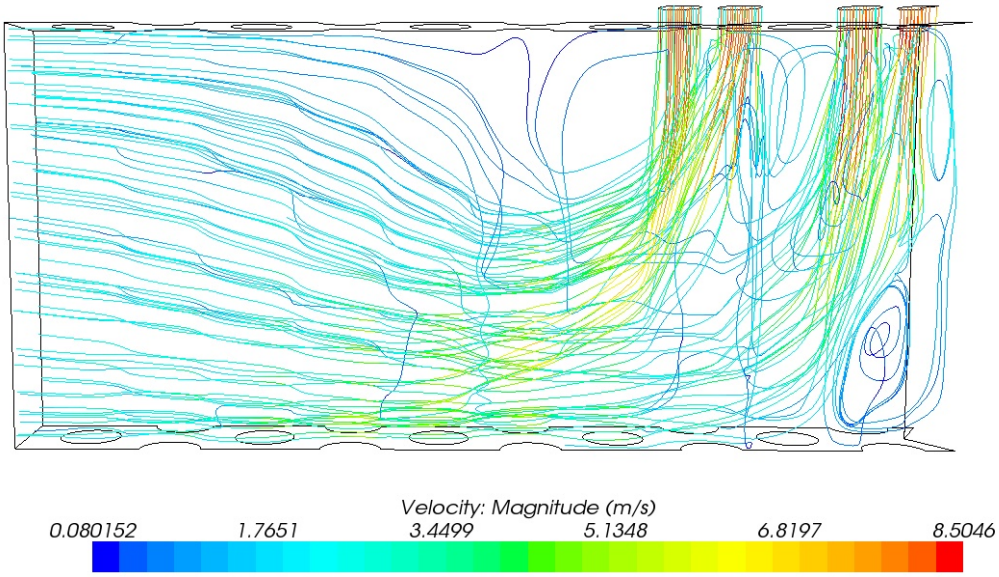

Figure 45. Streamline field computed for the 3D field at a point in time (1.27 seconds). The streamlines are colored by velocity magnitude.

Figure 46 is a photograph of a bubble visualization exercise where all four jets are injecting mineral oil into the physical model, but bubbles are being injected in the rightmost jet along with the liquid. It can be seen that flow patterns similar to the computed patterns in Figure 45 above are present. The flow is downward below the jets, then moves horizontally and somewhat upwards toward the exit at the left; there are zones of recirculation at the bottom right and between the two pairs of jets. There is also a large region of low speed flow and recirculation at the top center. The overall flow shown in Figures 45 and 46 appear to be intermediate between the first and third steady-state solutions of Figures 38 and 40 above.

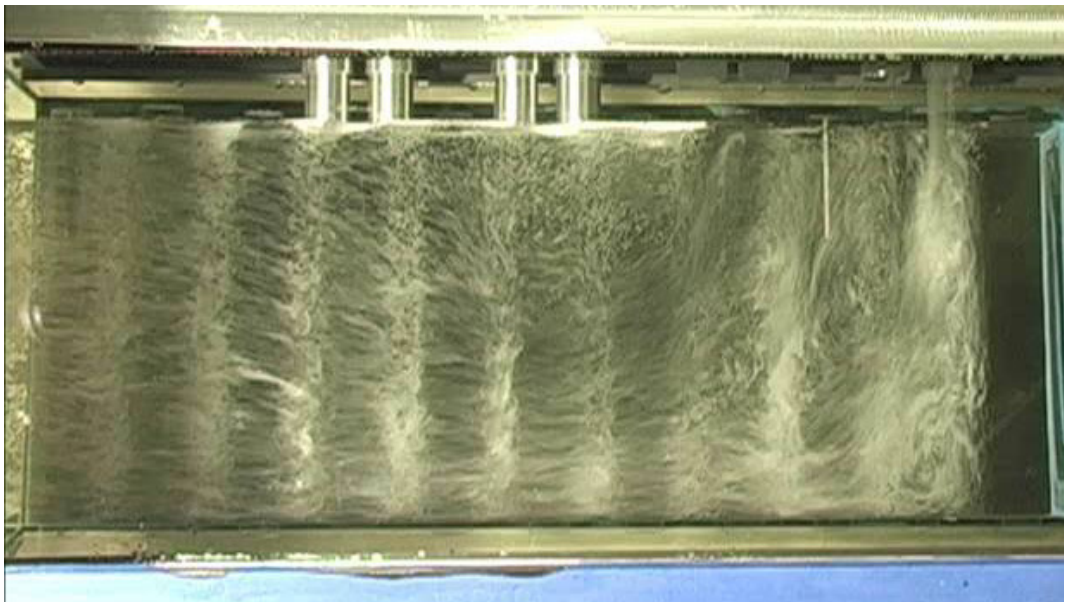

Figure 46. Photograph of a bubble visualization of the physical model of the Standard Problem. Bubbles are injected into the model through the rightmost jet; flow is right to left.

It is instructive to examine the time-varying streamwise velocity for a plane 150 mm below the inlet plane, or z = -150 mm. Figure 47 illustrates the streamwise velocity at this plane for a sequence of times.

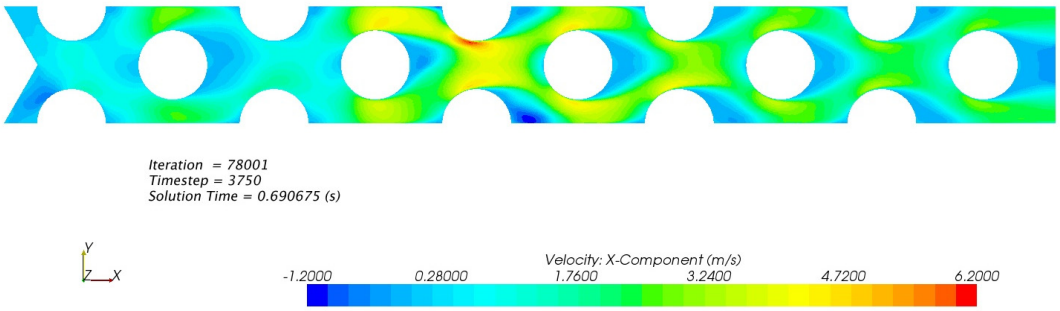

(a)

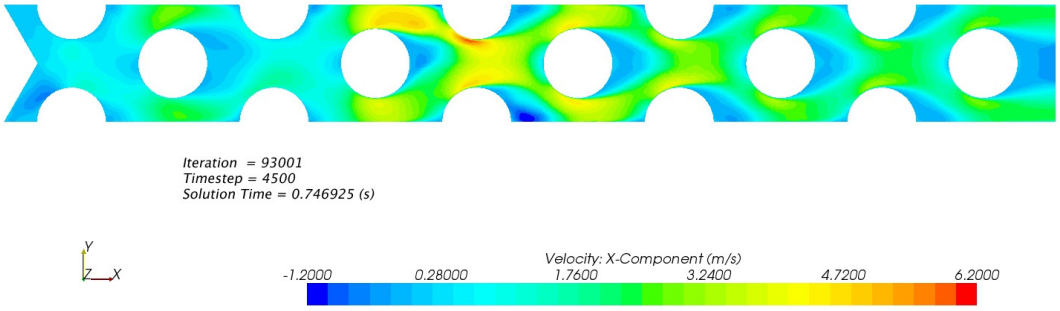

(b)

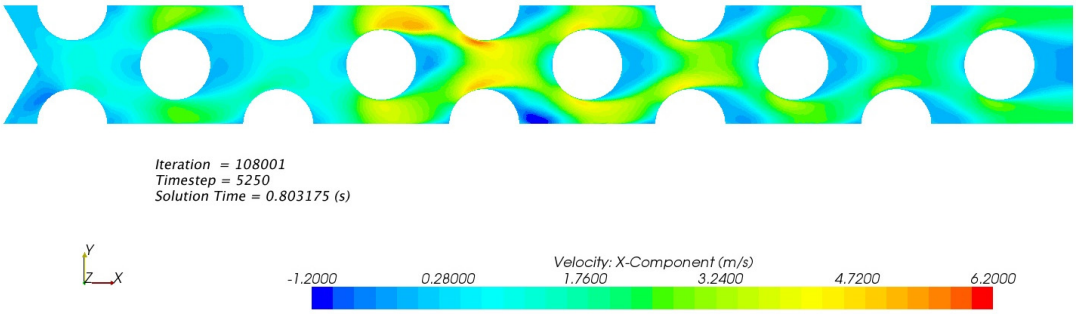

(c)

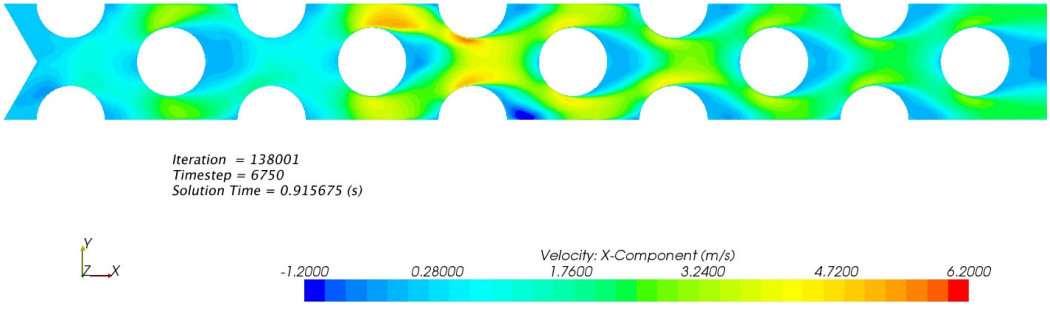

(d)

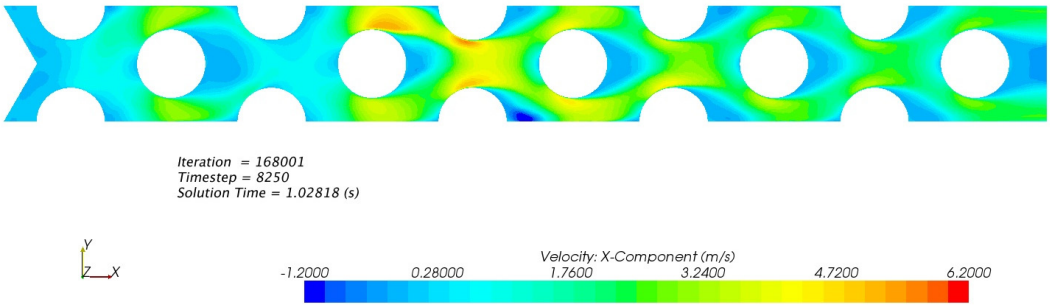

(e)

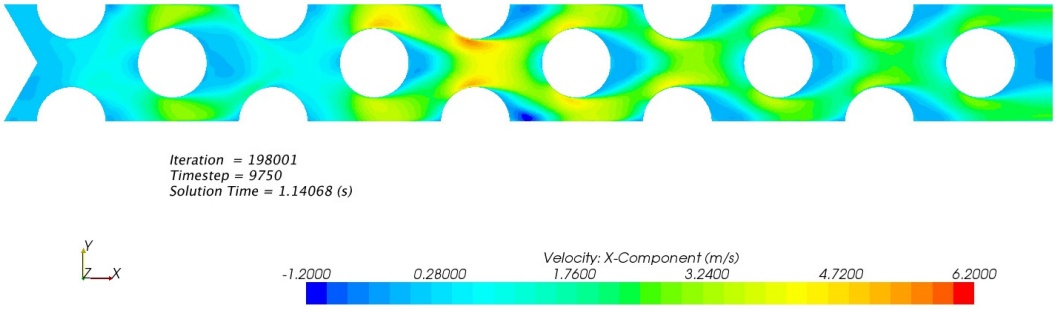

(f)

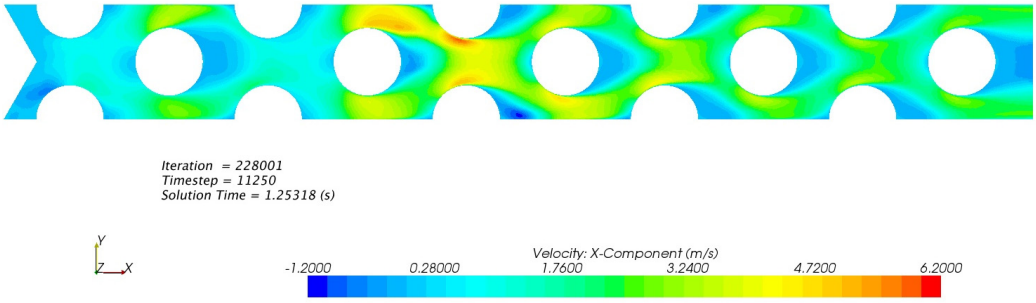

(g)

Figure 47. Time sequence of contour plots of the streamwise velocity at plane z = -150 mm. Times are given in the plots; the color scales are all synchronized to the same range.

An interesting pattern can be seen in the sequence of plots of Figure 47. If one examines the flow around the second full post from the left, one can see that the streamwise flow around the upper portion of the post (as displayed) increases in magnitude, then decreases, then increases again as a function of time. While it is not clear if vortices are being shed, what is clear is that the flow around the upper side of the post always has a higher magnitude than the flow around the lower side of the post. This indicates that the flow in not symmetric in the sense of a long-time average. This conclusion is reinforced by plotting the long-time average of the streamwise velocity at z = -150 mm. Figure 48 plots the mean or long-time average of the streamwise velocity at the same plane for time = 1.42 seconds. It is clear that the velocity preferentially flows around the top of the post, second from the left. Other asymmetries can be seen in the figure as well. While the actual inlet flow profiles are asymmetric because of the 90º-bend just upstream of the inlet ports, the asymmetries demonstrated in Figures 47–48 are not related to this asymmetry (because uniform inlet profiles are used). These asymmetries are caused by more subtle influences in the numerical simulations. They could be the result of the subtle asymmetry of the 3-D grid or of the

asymmetry of the initial flow as it chooses a preferential flow path during the initial steady flow computation.

This state of affairs is not desirable for a validation set. It is preferable that there is asymmetry in the mean flow, either because the inlet flow is highly asymmetric or because the geometry is deliberately designed to be asymmetric. Then, the flow would not be sensitive to very subtle influences that may be very difficult to replicate in a numerical simulation.

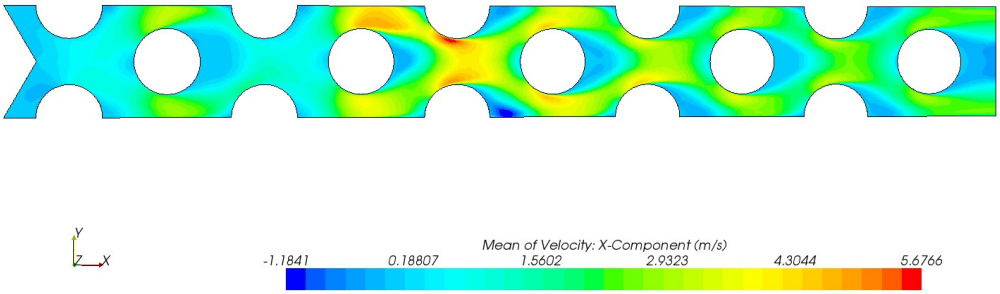

Figure 48. Long-time averaged (mean) streamwise flow velocity at z = -150 mm. Flow is asymmetric.

Even though more than 1.2 second of flow time was computed, it is apparently not the case that sufficient flow time has been achieved. (Flow times of several seconds were typically computed for the 2-D studies discussed above). Figure 49 plots the time-varying, Reynolds-averaged streamwise velocity at point p5. (See Figure 18 for x, y location of p5; z-location is at -150 mm.) It does not appear that enough flow time has been computed to obtain a state from which a meaningful long-time average can be calculated, although a repeating pattern may be emerging after t = 0.85 sec. This issue is better addressed by using a mesh with significantly fewer cells to allow results to be obtained more quickly.

In summary, the major flow features present in the actual flow are present in the computed flow. However, the CFD results exhibit asymmetries that are not related to the inlet profiles or the geometry, but are apparently caused by subtle influences. Also, additional compute time is necessary to determine if suitable long-time averages can be obtained for the flow for comparison with the experimental data. Computations using a coarser mesh may be useful to make further investigations into this and other issues. It is also desired to make computations using data-based inlet profiles to see if sufficient asymmetry is present to avoid excessive sensitivity of the flow to subtle influences.

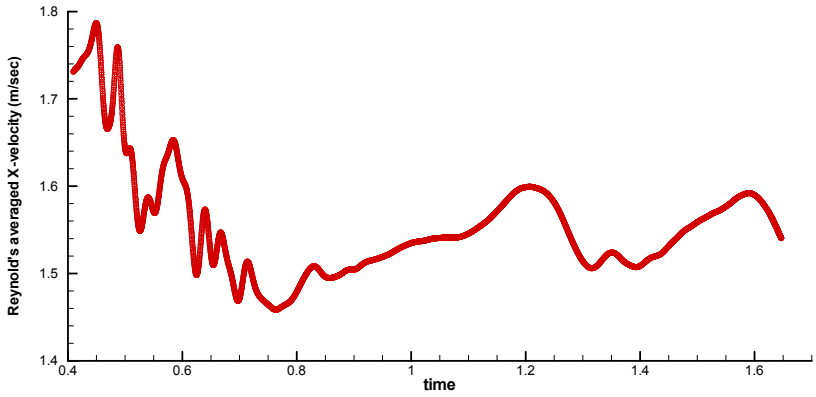

Figure 49. Time signature of the Reynolds-averaged streamwise velocity at point p5 in the 3-D flow field. Point p5 is located in the plane at z = -150 mm and in the same position as given by Figure 18.

4. ISSUES AND RECOMMENDATIONS

Several issues have been identified that may affect the suitability of the experimental data proposed to be a validation data set or Standard Problem. The following recommendations for the design of a new geometry for the purpose of generating a CFD validation data set are provided:

- ***Flow recirculation at the outlet of the physical model***. The calculations for the 2-D "inside-only" CFD model indicate that there is flow into the outlet of the CFD model. This is not a desirable situation because the true outlet conditions for this design are complex and therefore cannot be easily applied to an "inside-only" CFD model. Of course, an "inside-only" CFD model is by far the most desirable to minimize the number of cells in the computation. A remedy would be to make the physical model outlet farther downstream from where it currently is, with no additional posts included. Some calculations have been performed for a CFD model having an extended outlet that does not exhibit inflow at the outlet.

- ***Symmetry of the physical model***. 3-D calculations discussed earlier indicate that even when the geometry and inlet conditions for the CFD model are symmetric, asymmetry in the flow field can still occur. This is likely because of subtle asymmetries in the CFD model, such as the grid, or in the initialization of the CFD calculations, particularly when a pseudo-steady-state calculation is used as the initial condition for the unsteady calculations. The physical model should not be so sensitive to subtle influences that are difficult to replicate in the CFD model. It is desirable to deliberately build asymmetry into the physical model. It may still be the case that the inlet conditions, which are not symmetric, may be sufficient to provide clear asymmetry in the flow field. Further calculations still need to be made to investigate this possibility.

- ***Number of inlet jets in the physical model***. It is desirable to have only one inlet jet functioning in the physical model for two reasons. The first reason is that it is much easier to set up the problem with only one inlet condition, especially when detailed inlet data are used to provide several fields (three mean velocities and six turbulence stresses). The other reason is that if the desired asymmetry is provided by asymmetric inlet conditions, then it is prudent to have only one inlet to ensure that the asymmetry is preserved, rather than influenced by additional jets.

- ***Suitability of the geometry of the physical model***. The geometry of the physical model was designed to be an exact scaled portion of the lower plenum of the reference VHTR design. While this seems reasonable, it is more important to have a geometry that provides a suitable validation data set. The desirability of having only one jet has been discussed above. It seems unnecessary to include the "wedge" (seen at the left end of the model in the figures above) in the validation geometry; this likely adds no important physics to the flow. The presence of half posts in the geometry also seems to be undesirable in that full vortex shedding is not allowed to occur behind these wall-mounted structures. It appears better to have three or four rows of full posts with the wall moved somewhat away from the posts to allow full vortex shedding. Once the computational strategy has been developed and validated, the code can be applied to the actual geometry to see what happens therein. The numbers of posts should be kept to a reasonably small number to reduce the number of cells that would need to be contained in the associated computational mesh.

- ***CFD analyses of proposed validation geometry***. After a new geometry has been designed for a new validation data set, and before it is built, CFD simulations of the model should be made to see if there are any issues that would adversely affect its suitability for as a validation data set.

5. FUTURE WORK

The following recommendations are provided for future CFD computations related to the present physical model and to any design of a new model for use in generating a CFD validation data set:

- ***Coarser mesh calculations***. Inasmuch as the compute time for a 3-D unsteady flow can run into the hundreds of hours, it is desirable to create a coarser mesh than the one, described above, having 14 million cells. Such issues as the asymmetry of the actual inlet data for the present problem should be investigated to see if it is sufficient to definitively cause a preferential flow pattern that would not be very sensitive to subtle influences. Also, investigations should be undertaken into how long it takes to obtain a flow field that has some repeating pattern, which can then be long-time averaged to compare with the experimental data, which has also been long-time averaged. Other issues may also be identified and investigated in the course of the computations, which would be valuable to the analyst.

- ***Calculations using different meshes***. The nature of the mesh has an influence on the final computed results. There are a number of different types of meshes that can be and have been constructed using various types of mesh-generation software. Such meshes should be employed in unsteady 3-D computations to investigate the effects on the numerical solutions, including the effects on the near-wall treatments used by the particular turbulence model.

- ***Calculations for similar geometry at higher Reynolds number***. The Reynolds number for the present experimental data is known to be more than an order of magnitude smaller than that for the actual prismatic reference VHTR design. It might be useful to increase the Reynolds number of the CFD model to see if there are issues that arise because of a higher Reynolds number.

- ***Investigations into using laboratory CFD codes***. Department of Energy national laboratories have existing software that can be employed to perform CFD calculations. It would be desirable to investigate the application of such a code to see the advantages that might be available. Such advantages might include increased speed of computation, full control of the software for verification and validation purposes and knowledge of what is contained in the code, and the presence of more advanced algorithms in the code than are available in commercial CFD codes. One of the most important issues that presents itself to the CFD analyst for application to flow in a reactor vessel is the practicality of using CFD because of long compute times associated with meshes having large numbers of cells.

- ***Calculations for proposed new geometry***. As mentioned in a previous section, it is very desirable to make CFD calculations for any new geometry that is proposed for using to obtain a CFD validation data set.

6. REFERENCES

1. H. M. McIlroy, D. M. McEligot and R. J. Pink, Measurement of Flow Phenomena in a Lower Plenum Model of a Prismatic Gas-Cooled Reactor, Proceedings of the 16th International Conference on Nuclear Engineering (ICONE-16), Orlando, May 11-15, 2008.
2. FLUENT, version 6.3, 2008. FLUENT Inc., 10 Cavendish Court, Centerra Resource Park, Lebanon, NH, 03766.
3. http://journaltool.asme.org/Templates/JFENumAccuracy.pdf
4. R. W. Johnson, "Modeling Strategies for Unsteady Turbulent Flows in the Lower Plenum of the VHTR," Nuclear Engineering & Design, **238**, 482-491, 2008.
5. H. M. McIlroy, VHTR Lower Plenum 3D PIV Study, INL Laboratory Notebook LAB-184, pp. 105-148 of book 1 and 5-34 of book 2.
6. STAR-CD, version 4.06, 2008, CD-adapco, 60 Broadhollow Road, Melville, NY 11747.
7. STAR-CCM+, version 3.04, 2008, CD-adapco, 60 Broadhollow Road, Melville, NY 11747.
8. O. Simonin and M. Barcouda, 1986, "Measurements of Fully Developed Turbulent Flow across Tube Bundle," Proceedings of the Third International Symposium on Applications of Laser Anemometry to Fluid Mechanics, Lisbon, Portugal, 21.5.1-21.5.5.
9. O. Simonin and M. Barcouda, 1988, "Measurements and prediction of turbulent flow entering a staggered tube bundle," in: 4th International Symposium on Applications of Laser Anemometry to Fluid Mechanics, Lisbon, Portugal, paper 5.23.

Appendix A

Standard Problem Model Top View

Appendix A
Standard Problem Model Top View

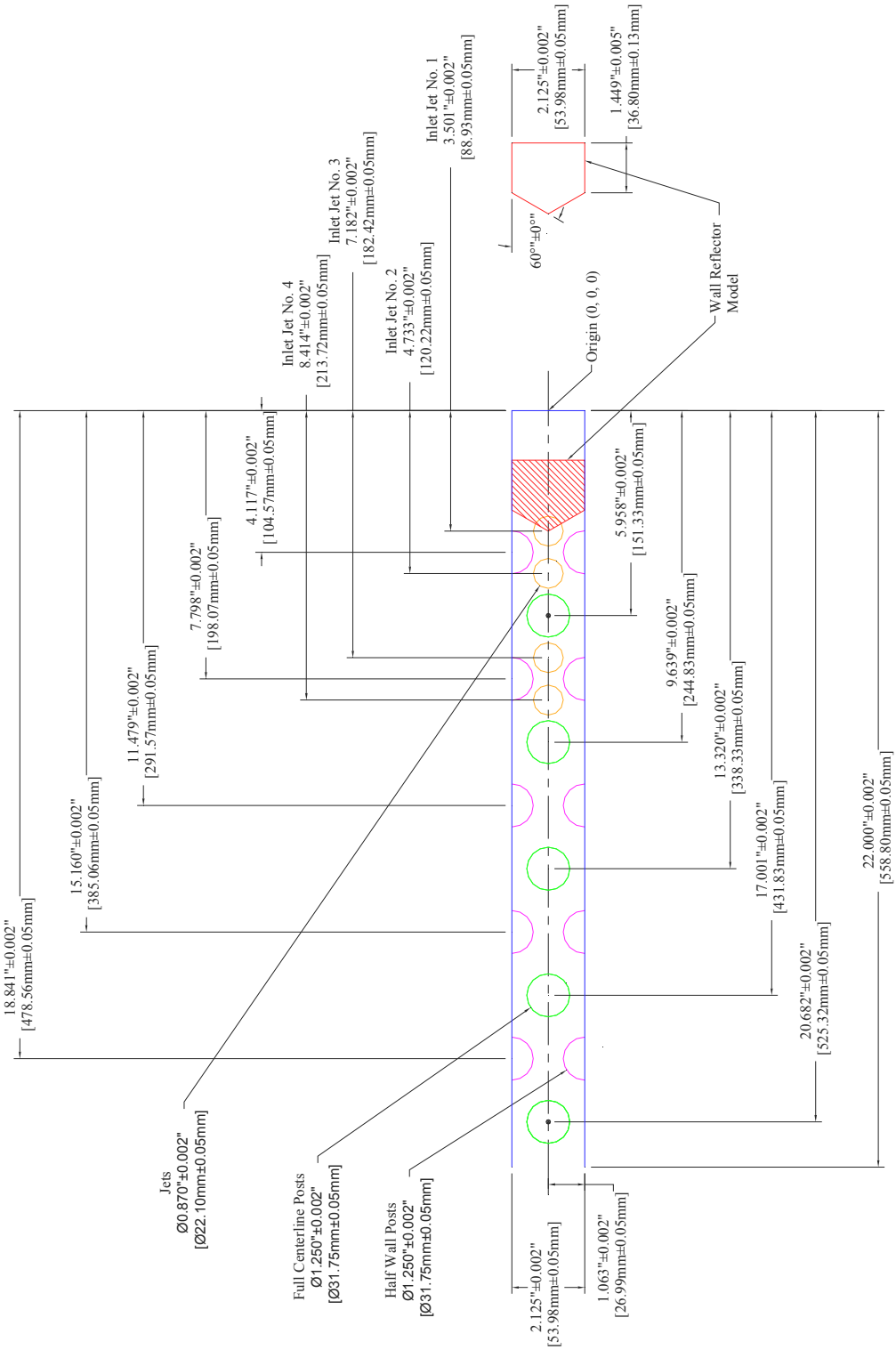

Standard Problem Model Front View

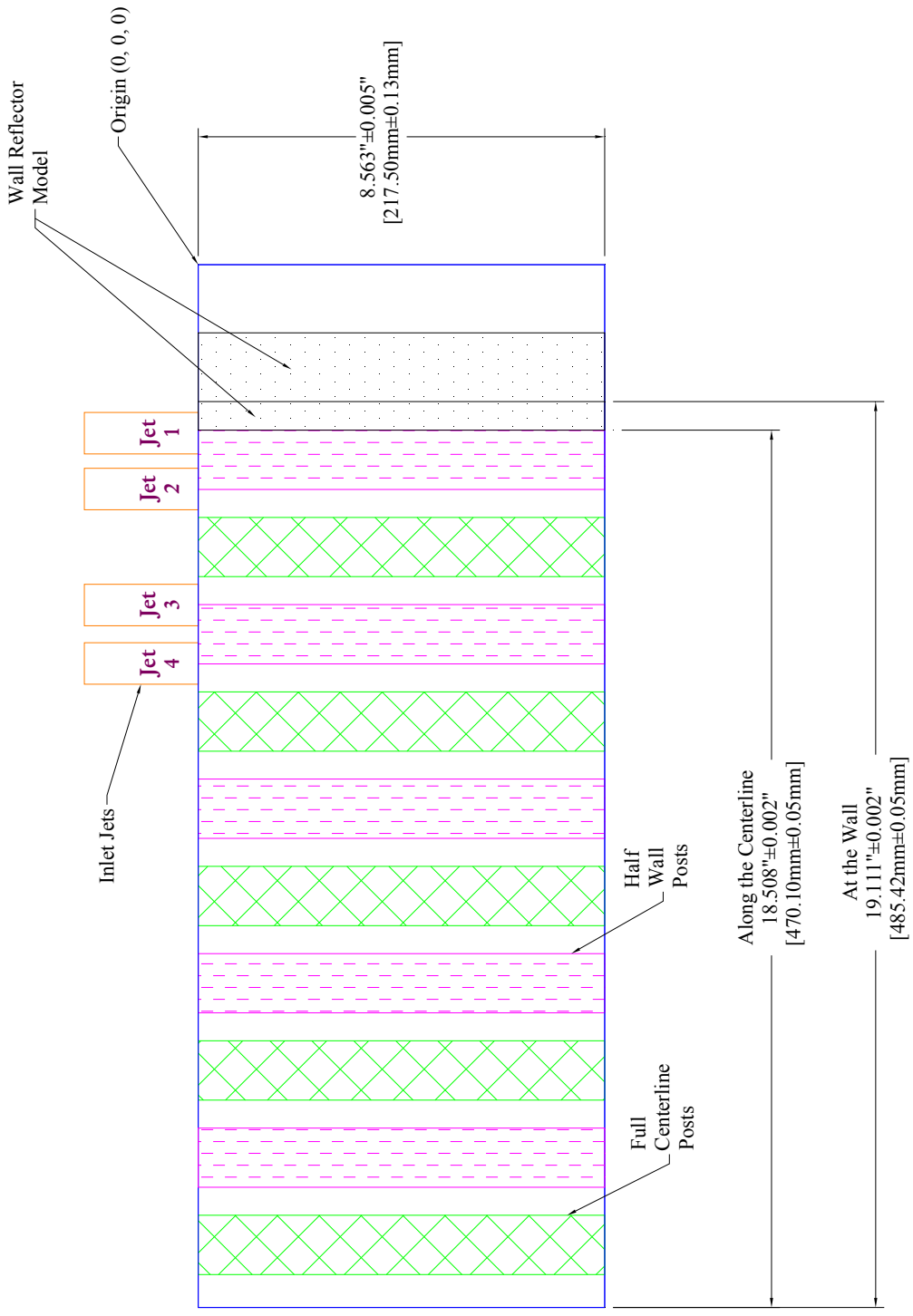

Appendix B

The Standard Problem Exercise

Appendix B
The Standard Problem Exercise

B-1. STANDARD PROBLEM EXERCISE

The Standard Problem exercise fits within the overall software qualification process outlined in Figure B-1. The entire process is described in some detail in the NGNP Methods Technical Program Plan.[1] That is, the Standard Problem exercise was defined on the basis of the need to characterize the flow behavior under operational conditions in the lower plenum of a prismatic reactor. The need was defined using the Phenomena Identification and Ranking Table (PIRT) process (Step 1). From this step, Matched Index of Refraction (MIR) experiments were defined and built to generate data to validate computational fluid dynamics (CFD) software. The data used as the basis for discussion and for the analyses shown in this report were measured in the MIR to achieve this purpose.

The validation process is centered in Step 2 of Figure B-1, where the process requires interactions with other entities to complete the validation objectives. To achieve a consensus that the selected MIR data are worthy of being a Standard Problem exercise, the data were introduced, described, and finally proposed to a Standard Problem Committee that resides within the Computational Methods, Validation and Benchmark (CMVB) Provisional Project Management Board (PMB) for Very High Temperature Reactors of the Generation IV International Forum. The Standard Problem Committee approved the proposal.[2]

Following approval by the Standard Problem Committee of the CMVB PMB, the NGNP Project has embarked on an effort to solicit Standard Problem exercise participants and to prepare the MIR data, geometry, essential information, and ground rules for transmittal to the participants. These efforts are briefly described below:

1. Prepare MIR Data for transmittal to Standard Problem participants.

   This effort was completed and the data are given in Reference 3. The data are contained in Appendix C of Reference 3.

2. Prepare ground rules, geometry, and essential information for transmittal to Standard Problem exercise participants.

   To complete the validation objective where it is important to demonstrate the capability of the software to calculate particular phenomena, the Standard Problem exercise must be rigorously defined, such that the Standard Problem participants all begin their analyses using the same ground rules, the same initial conditions, and the same boundary conditions. Consequently, the control volume of the analyses must be specified, the turbulence models of interest must be specified, the meshing requirements must be specified, the limits of the analyses must be prescribed, the computer requirements must be identified, and the time limits for the exercise must be defined. The results shown in this report summarize the work accomplished to date to establish the desired information for the participants in the Standard Problem exercise.

3. Solicitation of Standard Problem exercise participants

   Over the course of the past year, discussions have been held to determine the organizations that would likely participate in the Standard Problem exercise. To date, it appears that the following organizations will participate:

- CD-ADAPCO
- PBMR Pty

- Texas A&M University
- Nuclear Regulatory Commission
- West Virginia University.

It is hoped that the Standard Problem exercise will be initiated in Fiscal Year 2009.

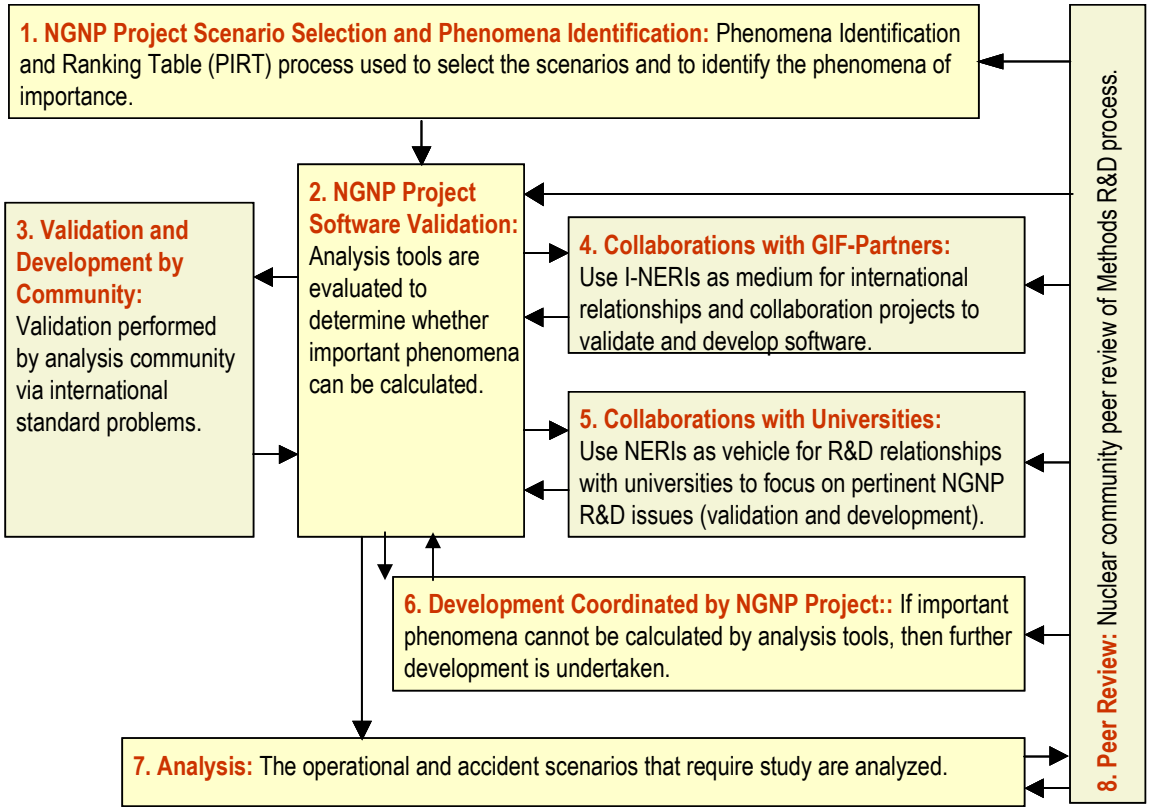

Figure B-1. Expanded description of methods R&D process.

B-1.1 Appendix B References

1. Schultz, R. R., Abderrafi M. Ougouag, David W. Nigg, Hans D. Gougar, Richard W. Johnson, William K. Terry, Chang H. Oh, Hugh M. McIlroy, Donald M. McEligot, Glenn E. McCreery, Woo Y. Yoon, James W. Sterbentz, Dana A. Knoll, J. Steve Herring, Temitope A. Taiwo, Thomas Y. C. Wei, William D. Pointer, Won S. Yang, Mitchell T. Farmer, Hussein S. Khalil, Madeline A. Feltus, C. P. Liou, "Next Generation Nuclear Plant Methods Research and Development Technical Program Plan," INL/EXT-06-11804, September, 2008.
2. Schultz, R. R. "Meeting Notes of Computational Methods, Validation and Benchmark (CMVB) Provisional Project Management Board (PMB) for Very High Temperature Reactors of the Generation IV International Forum," Miami, FL, July, 2006.
3. Schultz, R. R, Susan E. Krusch, Glenn E. McCreery, Hugh McIlroy, Chang H. Oh, D. Scott Lucas, M. T. Farmer, S. W. Lomperski, C. P. Tzanos, W. D. Pointer, T. Y. C. Wei, and C. P. Liou et al, "Next Generation Nuclear Plant Methods Thermal-Fluids Experiment Plan," INL/EXT-07-13289, September, 2007.

Appendix C

Table of CFD Code Features

Appendix C
Table of CFD Code Features

	STAR-CD v4.04	STAR-CCM+
Meshing Options		
Block Structured Mesh Generation Via Vertex Specification	Y	**N**
Automatic Mesh Generation		
Trimmed Cell	Y	Y
Trimmed Cell with Extrusion Layers	Y	Y
Polyhedral	Y	Y
Surface Wrapping	Y	Y
Surface Regeneration	Y	Y
Surface Smoothing	Y	Y
Mesh Smoothing	Y	Y
Adaptive Refinement (user iteration - not automated)	Y	**N**
Can import fluent, hexpress, harpoon and other mesher outputs	Y	Y
Solver Options		
Steady State		
SIMPLE	Y	Y
PISO	Y	**N**
Pseudotransient		
SIMPLE	Y	**N**
Transient		
segregated		
PISO		
fully-implicit first-order Euler Scheme	Y	**N**
SIMPLE		
fully-implicit first-order Euler Scheme	Y	Y
quadratic backward implicit	Y	**N**
Coupled		
Implicit	**N**	Y
Explicit	**N**	Y
Spatial Discretization Options		
Upwind Differencing	Y	Y
Linear Upwind Differencing	Y	Y
Central Differencing	Y	Y
Monotone Advection and Reconstruction Scheme	Y	Y
Heat Transfer		
Conjugate Heat Transfer	Y	Y
Radiation		

	STAR-CD v4.04	STAR-CCM+
Discrete Transfer Method	Y	Y
Discrete Ordinates	Y	**N**

Solid Mechanics		
Finite Volume solution of stress and strain	Y	N
Turbulence Models		
One Equation Models		
Mixing Length	Y	Y
Spalart-Allmaras (with and without wall function)	Y	Y
Two-Equation Linear		
Single Layer		
High-Re k-epsilon Model	Y	Y
Chen	Y	N
RNG	Y	N
V2F relaxation model	Y	Y
Low-Re k-epsilon	Y	Y
High-Re Realizable k-epsilon	N	Y
Low-Re Realizable k-epsilon	N	Y
AKN	N	Y
Wilcox k-omega	Y	Y
k-omega SST	Y	Y
k-omega BSL	N	Y
Two Layer		
High-Re k-epsilon Model	Y	Y
High-Re Realizable k-epsilon Model	N	Y
Two-Equation Non-Linear		
quadratic High and Low Re k-epsilon	Y	N
cubic High and Low Re k-epsilon	Y	N
cubic and quadratic Suga (high Re)	Y	N
cubic and quadratic Speziale (high Re)	Y	N
Reynolds Stress		
Gibson Launder (Linear)	Y	Y
SS&G (Quadratic)	Y	Y
Linear Two layer	Y	Y
LES		
Smagorinsky	Y	Y
DES		
Spalart-Allmaras	Y	Y
k-omega SST	Y	Y